Bulletin of Earthquake Engineering
https://doi.org/10.1007/s10518-023-01813-9

ORIGINAL ARTICLE

Design displacement for lifelines at fault crossings: the code-based approach for Europe

Vasileios E. Melissianos[1] · Dimitrios Vamvatsikos[1] · Laurentiu Danciu[2] · Roberto Basili[3]

Received: 23 December 2022 / Accepted: 29 October 2023

Abstract
The earthquake-resistant design of lifelines, such as pipelines, tunnels and bridges, is based on the reliable representation and estimation of the seismic loading. In the case of lifeline–fault crossings, the design fault displacement is typically derived from estimates based on fault dimensions via empirical fault scaling relations for a given "design" scenario event. This approach comes with an unknown level of safety because the fault productivity and the actual distribution of earthquake events are essentially disregarded. To overcome this challenge, a simplified approach is proposed by statistically analyzing the outcome of probabilistic fault displacement hazard analyses (PFDHAs). A selection of faults from the 2020 European Fault-Source Model is used to build the logic tree and to set the range of parameters considered in the PFDHAs. The methodology allows the (mostly conservative) approximation of the fault displacement corresponding to any given return period based on readily available data, namely fault productivity, fault mechanism, fault length, and lifeline crossing location on the fault. The proposed methodology has been proposed and adopted as an informative Annex in prEN 1998-4:2022.

Keywords Lifelines · Fault crossing · Design fault displacement · Uncertainties · Eurocodes

Abbreviations and symbols

EFSM20	2020 European fault-source model
ESHM20	2020 European seismic hazard model
INT	Interplate tectonic environment
MAF	Mean annual frequency
PFDHA	Probabilistic fault displacement hazard analysis
SCR	Stable continental region tectonic environment

✉ Vasileios E. Melissianos
melissia@mail.ntua.gr

[1] School of Civil Engineering, National Technical University of Athens, Heroon Polytechneiou 9, Politechneioupoli, 15772 Zografos, Attica, Greece

[2] Swiss Seismological Service, ETH Zurich, Sonneggstrasse 5, 8092 Zurich, Switzerland

[3] Istituto Nazionale di Geofisica e Vulcanologia, Via di Vigna Murata 605, T00143 Rome, Italy

C_F	Confidence factor
L_F	Fault length
M or m^*	Earthquake (moment) magnitude
PoE	Probability of exceedance
$S_{\beta,475}$	Design spectral acceleration at period $T_\beta = 1$ s corresponding to a return period of 475 years per EN1998-1-1:2021
T_R	Return period
X_L	Normalized distance of lifeline–fault crossing point from closest fault end
b	b-Value of Gutenberg–Richter law
v_F	Recurrence rate of all earthquakes on fault above a minimum magnitude
$v_{F,approx}$	Approximated recurrence rate
$v_{F,approx,u}$	Updated approximated recurrence rate with confidence factor
ε	Residuals of fitted model
λ_{Δ_F}	Mean annual frequency of fault displacement at lifeline crossing site
σ_ε	Root mean square error of fitted model (prediction error)
Δ_F or $\delta_F{}^*$	Fault displacement at lifeline crossing site
*	lowercase letter denotes the value of the variable with uppercase letter

1 Introduction

The structural integrity and functionality of critical infrastructure, such as oil, gas, water, and sewage pipelines, as well as roads, tunnels, and bridges in the aftermath of an earthquake is decisive for the management of response actions by the civil protection authorities and heavily influences the seismic resilience of communities (Casari and Wilkie 2005; Fragiadakis et al. 2015; Kilanitis and Sextos 2019; Mazumder et al. 2020). A potential failure may result in injuries and human fatalities, environmental pollution, as well as significant direct and indirect economic losses (Somerville 1995; Basöz et al. 1999; Bird and Bommer 2004; Steinberg and Cruz 2004; Nair et al. 2018). Even though strict standards are applied during the design, construction, operation, and maintenance of these critical infrastructures, failures are still occurring. Among the most catastrophic earthquake-induced actions is the fault offset in case of large-magnitude earthquakes affecting the overlying structures. Fault offset is the differential displacement along a fault plane in the earth's crust, appearing wherever the causative fault rupture propagates up to the ground surface. Any structure subjected to fault offset has to follow the ground displacement by developing excessive deformations. This has been studied for buried pipelines (Girgin and Krausmann 2016), above-ground pipelines (Honegger et al. 2004), pipeline networks (O'Rourke 2010; O'Rourke et al. 2014), tunnels (Roy and Sarkar 2017), and bridges (Anastasopoulos and Gazetas 2007; Yang and Mavroeidis 2018).

The seismic resilience of critical lifelines and infrastructure against tectonic faulting can be secured within the framework of Performance-Based Earthquake Engineering (Cornell and Krawinkler 2000), which requires at first the quantification of the fault displacement hazard at the crossing site. The most appropriate methodology to do so is the Probabilistic Fault Displacement Hazard Analysis [PFDHA (Youngs et al. 2003; Moss and Ross 2011; Petersen et al. 2011; Valentini et al. 2021)]. A comprehensive framework for the performance assessment of buried pipelines at fault crossings has been presented by Melissianos et al. (2017), which was further refined and focused on the fault displacement hazard at lifeline–fault crossings on an engineering basis by Melissianos et al. (2023). PFDHA aims at quantifying the mean annual frequency of exceeding arbitrary fault displacement levels

at the lifeline crossing site, considering the dimensions and the seismological properties of the fault along with the location of the crossing lifeline on the fault trace (i.e., the crossing site). However, this is an advanced analysis with complicated probabilistic calculations based on a set of specialized seismological data [see for example the site-specific analysis for the Milun Fault in Taiwan recently published by Gao et al. (2022)] and thus unsuitable for being incorporated "as is" in code provisions.

In response, a code-compatible statistical approximation is developed for estimating the design fault displacement for application across Europe. A large number of PFDHAs was executed considering the pertinent uncertainties within a logic tree framework (Bommer and Scherbaum 2008) to handle the seismological and geometrical properties of faults obtained from the 2020 European Fault-Source Model [EFSM20 (Basili et al. 2022)] that was used for the development of the 2020 European Seismic Hazard Model [ESHM20 (Danciu et al. 2021)]. Further, the PFDHA results were statistically analyzed and a procedure for estimating the fault displacement was developed.

The main outcome of this study is a set of empirically-derived equations that establish a link between the fault displacement and key variables, such as the fault seismic productivity, the fault mechanism, the fault length, and the crossing point on the fault trace. These expressions constitute an engineering orientated and code-compatible methodology that allows the estimation of the design fault displacement for lifelines crossing active tectonic faults. This methodology is a structure-independent and hazard-consistent approach that is applicable by engineers, who are typically not familiar with detailed hazard calculations, as well as specialized seismological and geophysical data. The proposed methodology has been adopted in prEN 1998-4:2022 (European Committee for Standardisation 2022) as an informative Annex. It is important to emphasize that the methodology described should not be considered a substitute for a comprehensive assessment of fault displacement hazard specific to the site in question, particularly in cases involving high-risk infrastructure or when such an assessment is explicitly mandated by the owner of the infrastructure or regulatory authorities.

2 Proposed methodology

The proposed methodology for estimating the design fault displacement, referred as the EN1998-4 approach hereinafter, is implemented as follows:

1st step: The fault mechanism, the fault length, and the crossing point are determined for the lifeline-fault crossing at hand. In more detail:

- The fault mechanism determines the mechanical response of the fault-crossing structure. For example, the deformation of a buried pipeline subjected to normal, reverse, and strike-slip faulting is depicted in Fig. 1. Normal faulting causes pipe bending and elongation, reverse faulting causes pipe bending and shortening, while strike-slip faulting causes

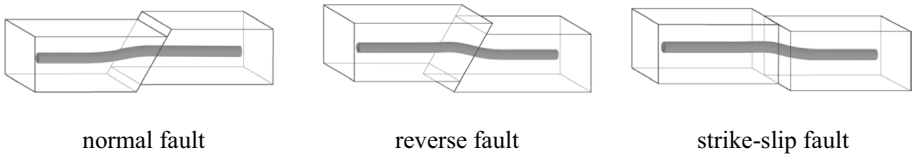

Fig. 1 Fault mechanisms and corresponding pipe deformation (the right block is the stationary, while the left is the moving one)

pipe bending (O'Rourke and Liu 2012). At this point, it shall be noted that the effect of fault trace uncertainty related to the propagation of rupture through soil until reaching the ground surface (e.g., Anastasopoulos et al. 2007, 2008; Loukidis et al. 2009) is not considered.

- The fault (subsurface) length (L_F) can be obtained from a geological map or defined by an appropriate survey.
- The crossing point (X_L) stands for the ratio of the distance along the fault trace of the lifeline–fault crossing point to the closest fault-end over the fault trace length as per Fig. 2; naturally $0 < X_L \leq 0.50$. The crossing point itself results from the lifeline route selection procedure.

2nd step: The recurrence rate (v_F) of the fault, representing the earthquake occurrence, is the average annual rate of all earthquakes above a minimum magnitude and is derived either from an available source model or defined by a specialized seismological study. The minimum earthquake magnitude considered is 5.5, assuming that lower magnitudes do not cause enough fault displacement to endanger the lifeline integrity. Alternatively, the recurrence rate can be approximated ($v_{F,approx}$) via the proposed methodology presented in Sect. 5 using the fault length (L_F) and the the reference spectral acceleration at period $T_\beta = 1$ s corresponding to a return period of $T_R = 475$ years (as estimated via ESHM20) at the crossing site. The recurrence rate is classified into two categories as per Table 1.

3rd step: The return period (T_R) of exceeding a selected fault displacement level at the lifeline–fault crossing is estimated as:

$$T_R\left(\Delta_F\right) = \frac{1}{C_F v_F f_L\left(\Delta_F, L_F, X_L\right)} \tag{1}$$

with $0.25\,\text{m} \leq \Delta_F \leq 4.00\,\text{m}$ where: C_F is the confidence factor estimated after Eq. (3), v_F is the recurrence rate obtained from the 2nd step, $f_L\left(\Delta_F, L_F, X_L\right)$ that depends on the fault

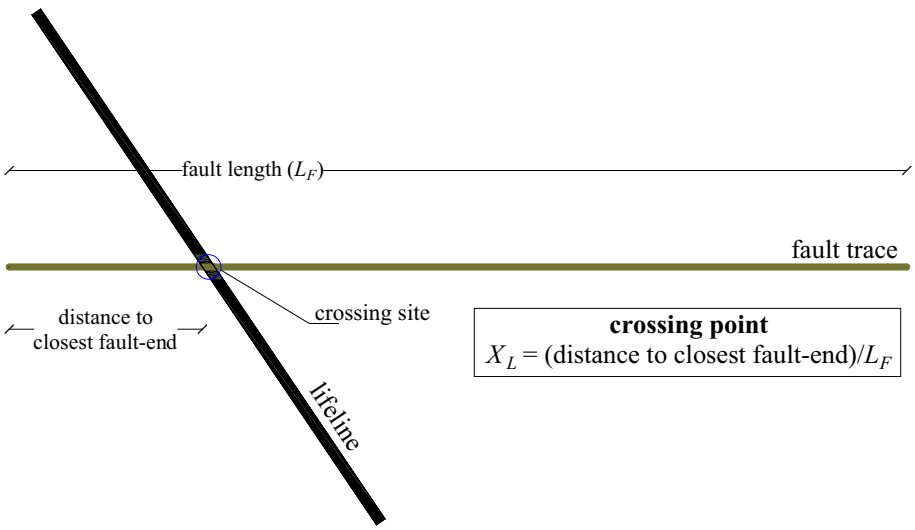

Fig. 2 Lifeline–fault crossing plan view

Table 1 Recurrence rate (v_F) classification

Class	Range in year^{-1}
Low	$v_F \leq 0.10$
High	$v_F > 0.10$

mechanism, fault length, and crossing point; estimated for the selected fault displacement after Eq. (2) based on the recurrence rate classification of Table 1.

$$f_L\left(\Delta_F, L_F, X_L\right) = \exp\left[\begin{array}{l} a_1 + a_2 \ln L_F + a_3 X_L + a_4\left(\ln L_F\right)^2 + a_5 X_L \ln L_F + \\ a_6 {X_L}^2 + a_7\left(\ln L_F\right)^3 + a_8 X_L\left(\ln L_F\right)^2 + a_9 {X_L}^2 \ln L_F \end{array}\right] \quad (2)$$

where ln(•) is the natural logarithm of its argument and the coefficients a_1, a_2, …, a_9 differ per recurrence rate class and Δ_F value, as listed in A1 for normal fault, in Table A2 for reverse fault, and in Table A3 for strike-slip fault mechanism

The confidence factor C_F is estimated as:

$$C_F = \begin{cases} 1.00 & \text{for } v_F \\ \text{Eq. (12)} & \text{for } v_{F,approx} \end{cases} \quad (3)$$

The following remarks should be additionally considered:

1. If there is uncertainty about the crossing point, then $X_L = 0.50$ should be considered as the worst-case scenario because it yields a higher MAF of exceeding any fault displacement (Melissianos et al. 2023).
2. In case the fault displacement corresponding to a design return period is requested, as it is typically the case in design applications and it is the inverse of what is obtained from Eq. (1), linear interpolation in $\left[\Delta_F, \ln T_R\left(\Delta_F\right)\right]$ space may be employed among the values estimated after Eq. (1) as per Fig. 3.
3. If the obtained fault displacement value is outside the range of Eq. (1), namely $\Delta_F < 0.25$ m or $\Delta_F > 4.00$ m, then linear extrapolation in the $\left[\Delta_F, 1/\ln T_R\left(\Delta_F\right)\right]$ space may be employed as a conservative option (Fig. 4). If values lower than 0.10 m are obtained, then it is suggested to consider $\Delta_F = 0.10$ m as a minimum design value for safety reasons. If values significantly higher than 4.00 m are estimated, then a more detailed site-specific seismological study should be performed.
4. If the approximated recurrence rate has been employed (see Sect. 5), then the design fault displacement value should be the minimum between the one obtained via the interpolation of Fig. 3 and the deterministic cap of Table 2. The deterministic cap is roughly the 90% percentile of the empirical fault scaling relations of Leonard (2014) that relate the average fault displacement with the fault length.
5. Only principal faulting is considered, while any additional differential displacement appearing at sites away from the fault trace due to distributed/secondary faulting (i.e., displacements, shear, fractures, etc. located up to a few kilometers from the principal fault) is neglected.

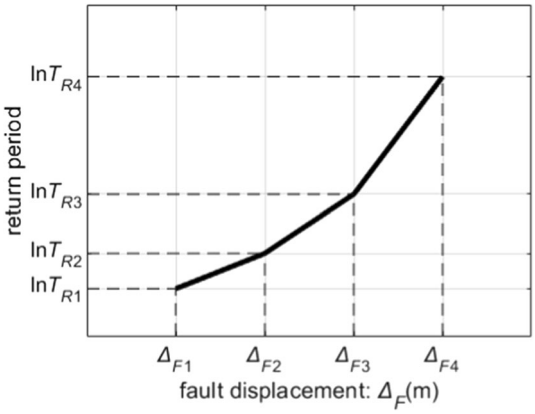

Fig. 3 Determination of the $\ln T_R(\Delta_F)$ versus Δ_F relationship via linear interpolation (T_R in years)

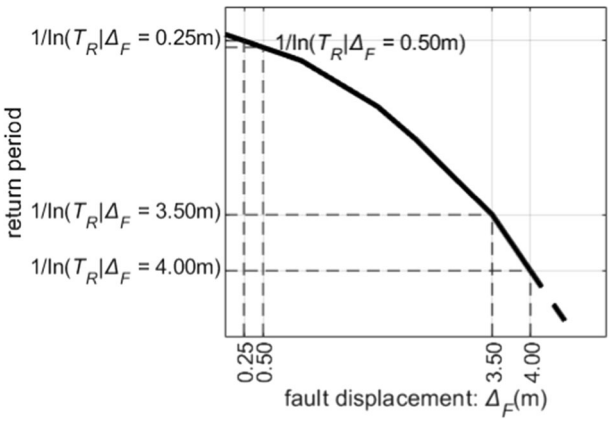

Fig. 4 Linear extrapolation of the $1/\ln T_R(\Delta_F)$ versus Δ_F relationship for fault displacement $\Delta_F < 0.25$ m and $\Delta_F > 4.00$ m (T_R in years)

Table 2 Fault displacement deterministic cap ($\Delta_{F,det.cap}$)

Fault mechanism	Fault displacement cap ($\Delta_{F,det.cap}$ in m and L_F in km)
Normal	$\Delta_{F,det.cap} = 0.182 {L_F}^{0.833}$
Reverse	$\Delta_{F,det.cap} = 0.182 {L_F}^{0.833}$
Strike-slip	$\Delta_{F,det.cap} = 0.130 {L_F}^{0.833}$ for $L_F \leq 40$ km
	$\Delta_{F,det.cap} = 0.451 {L_F}^{0.500}$ for $L_F > 40$ km

3 Methodology background

3.1 Fault displacement hazard calculation

The (mostly) rate-independent function $f_L(\Delta_F, L_F, X_L)$ of Eq. (2) has been derived from the statistical processing of a large number of PFDHA results that were carried out

using the baseline engineering approach developed by Melissianos et al. (2017, 2023). In particular, PFDHA yields the mean annual frequency (MAF) of exceeding a predefined fault displacement (δ_F) on the lifeline crossing site, calculated as:

$$\lambda_{\Delta_F}(\delta_F) = \nu_F PoE \tag{4}$$

where the probability of exceeding (PoE) a given fault displacement value is:

$$PoE = \sum\nolimits_i P(\Delta_F > \delta_F | m_i) P_M(m_i) \tag{5}$$

$P(\Delta_F > \delta_F | m_i)$ the conditional probability that fault displacement Δ_F will exceed value δ_F given an earthquake of magnitude m_i has occurred and $P_M(m_i)$ is the probability of the earthquake magnitude M being in a bin of $m_i \pm \Delta m$, provided that M ranges between a minimum (M_{min}) and a maximum (M_{max}) value. $P_M(m_i)$ is estimated after the Gutenberg–Richter (G-R) bounded recurrence law (Gutenberg and Richter 1944):

$$P_M(m_i) = P(M < m_i + \Delta m | M_{min} \le m_i \le M_{max}) - P(M > m_i - \Delta m | M_{min} \le m_i \le M_{max})$$

with:

$$P(M < m_i | M_{min} \le m_i \le M_{max}) = \frac{1 - \exp[-b(m_i - M_{min})]}{1 - \exp[-b(M_{max} - M_{min})]} \tag{6}$$

where the b-value is the slope of the curve that provides the "expected" future earthquake magnitudes and is a seismological property of the fault.

The main input for performing the fault displacement hazard calculations is:

- fault mechanism and length, which are available to the engineer from a geological map or a seismic source model,
- the b-value of the G-R law and the maximum earthquake magnitude (M_{max}), which are specialized seismological information, being estimated by other specialists and not engineers,
- and the crossing point, which is defined from the lifeline route selection procedure (e.g., Seel et al. 2014; Hamid-Mosaku et al. 2020).

The fault mechanism, fault length, and the crossing point are direct input parameters for the proposed methodology (Sect. 2), while the b-value of the G-R law and the maximum earthquake magnitude were considered as epistemic uncertainties related to the model parameters and were handled through logic trees (Bommer and Scherbaum 2008).

3.2 Database of active faults

A selection from the ESFM20 database of seismically active faults (Basili et al. 2022) that was created for the development of ESHM20 (Danciu et al. 2021) was exploited through a data mining process. The aim was to identify the main properties of the faults in order to (1) define the range of parameters (fault mechanism, tectonic environment, fault length) for examination and (2) develop the appropriate logic trees for handling the uncertainties on variables. It is noted that for engineering purposes, we excluded from the analysis

faults with length $L_F < 10$ km and $L_F > 300$ km, as well as (blind) faults whose uppermost boundary is located deeper than 3 km from the surface.

3.2.1 Tectonic environment and fault mechanism

The faults examined are mapped in Fig. 5, distinguished by tectonic environment between Interplate (INT) and Stable Continental Region (SCR). A statistical analysis of the number of faults per tectonic environment and mechanism, separately, is shown in Fig. 6. The vast majority of faults are INT (94%) compared to SCR ones (6%). Regarding the fault mechanism, nearly half of the faults are normal, while reverse faults are the fewest.

3.2.2 Gutenberg–Richter law *b*-value

The G-R law is an integral part of the fault displacement hazard calculation (Kramer 1996) and even though it was developed in the 1940s, it remains a standard tool for estimating the magnitude of future earthquakes (Bommer 2002). The *b*-value is a

Fig. 5 Map of faults classified per tectonic environment (INT: red, SCR: blue), a selection from the EFSM20 database (Danciu et al. 2021; Basili et al. 2022)

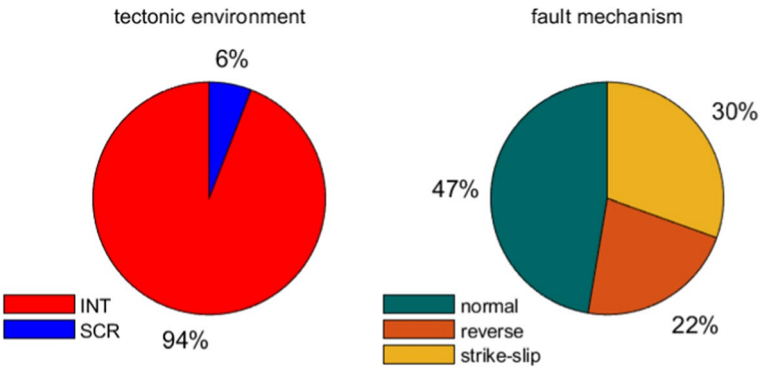

Fig. 6 Tectonic environment and mechanism of examined faults [a selection from the EFSM20 database (Danciu et al. 2021; Basili et al. 2022)]

seismogenic parameter and is the negative slope of the recurrence curve expressing the average ratio of exponentially distributed small and large magnitude earthquakes (Danciu et al. 2021) and affects the shape of the fault displacement hazard curve at the crossing site (Melissianos et al. 2023). In ESHM20, a single *b*-value is used for each active tectonic fault, since the sensitivity analysis revealed that the uncertainty of *b*-value has lower impact on the magnitude-frequency-distributions compared to the fault slip-rates and M_{max} uncertainties. The *b*-values were calculated via a set of complex procedures presented in the documentation of ESHM20, being related to the declustering of catalogues of recorded earthquakes.

The distribution of *b*-values per tectonic environment is presented in Fig. 7, where it is revealed that the predominant value is $b = 1.00$, while the number of faults with $b > 1.00$ is much lower than those with $b < 1.00$. The same conclusions are drawn regarding the distribution of *b*-values per fault mechanism (Fig. 8).

3.2.3 Earthquake recurrence rate

The earthquake recurrence rate of a fault provides the average annual number of events above the minimum earthquake magnitude of engineering significance, M_{min}. The value $M_{min} = 5.5$ is adopted on the basis of engineering and scientific judgement and since

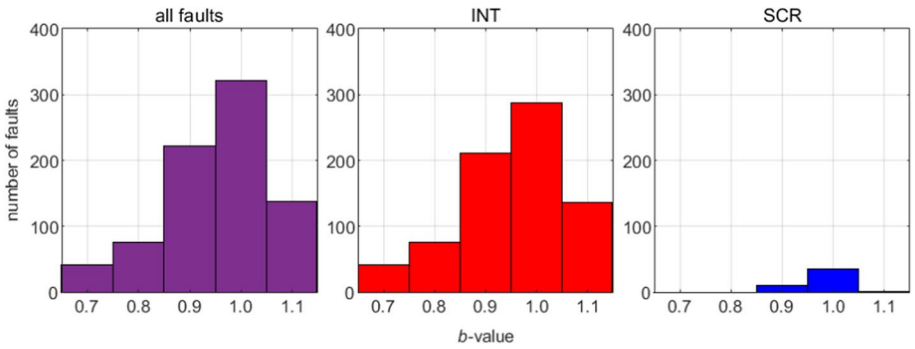

Fig. 7 Histograms of G-R *b*-value per tectonic environment

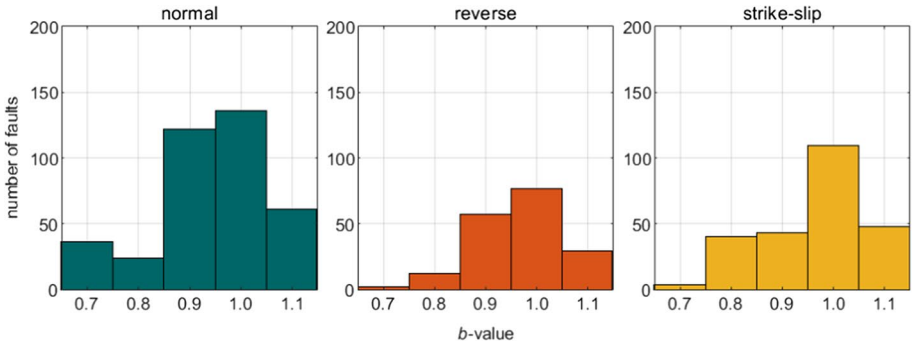

Fig. 8 Histograms of G-R *b*-value per fault mechanism

the resulting fault displacement for lower magnitude values is insignificant. The latter is based on the effect of the conditional probability of slip that is an integral part of PFDHA and represents the probability of the rupture reaching the surface, conditioned only on earthquake magnitude. For all three fault mechanisms, a magnitude $M > 5.50$ event is required to have at least 20% probability for the rupture to even reach the surface (Melissianos et al. 2023).

The rate of events with magnitude higher than M_{min} is estimated via the formula:

$$v_F\left(M > M_{min}\right) = 10^{a-bM_{min}} \tag{7}$$

where the a-value (representing the total seismic productivity of a given fault) and the b-value (Sect. 3.2.2) can be obtained from a site-specific geological study or (in our case)

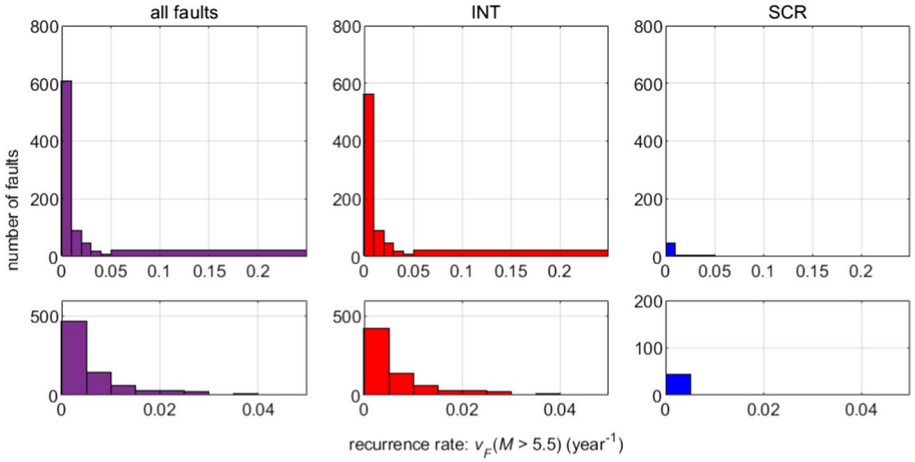

Fig. 9 Histograms of earthquake recurrence rate values, $v_F(M > 5.5)$, of faults per tectonic environment (top row: full range of rate values, bottom row: rates lower than 0.05 year^{-1})

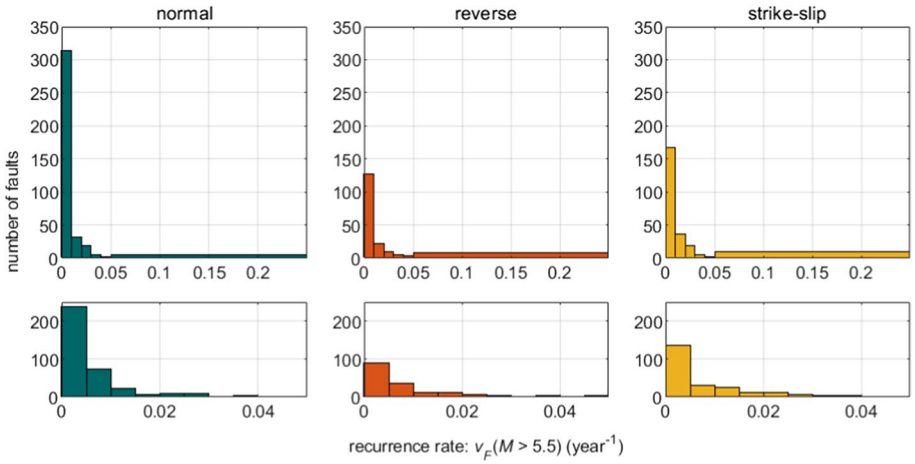

Fig. 10 Histograms of earthquake recurrence rate values, $v_F(M > 5.5)$, of faults per mechanism (top row: full range of rate values, bottom row: rates below 0.05 year^{-1})

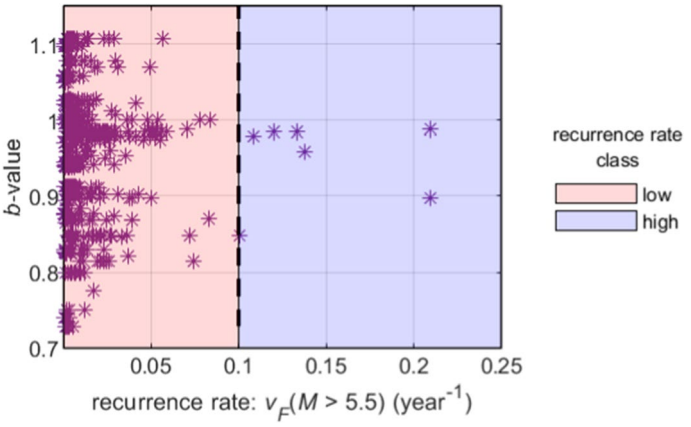

Fig. 11 b-value versus $v_F(M > 5.5)$ and definition of recurrence rate classes

the EFSM20. The resulting rate for each fault of the database has been estimated and the results are presented in Fig. 9 per tectonic environment. As expected, the rate of SCR faults is much lower compared to the more active INT faults. The distribution of rates per fault mechanism is depicted in Fig. 10, indicating a significant scattering of values.

3.3 Handling of uncertainties

The epistemic uncertainties related to the model parameters, namely the b-value of the G-R law and the maximum earthquake magnitude, are handled through logic trees. Additionally, provided that the SCR faults are few compared to the INT ones, the tectonic environment is also treated as an epistemic uncertainty due to the involvement of expert judgment and sometimes subjective definition. Every logic tree branch leads to an alternative scenario or, in other words, to a different mean annual frequency (MAF) of exceeding a predefined fault displacement.

3.3.1 Logic tree of Gutenberg–Richter b-value

The b-value is related to the earthquake recurrence rate v_F, as depicted in Fig. 11 for the active faults of the database. Therein, the earthquake recurrence rate is plotted on the horizontal axis and the b-value on the vertical one. The two recurrence rate classes (Table 1) are also presented, with their boundary defined empirically based on a direct search for optimal classification.

A further breakdown of Fig. 11 per tectonic environment and fault mechanism is provided in Fig. 12. Regarding the tectonic environment, SCR faults could be found only in the low recurrence rate class, as should be expected. Also, significant scattering of the values with respect to the fault mechanism was detected and consequently, it was decided to handle the b-values in each recurrence rate class independently per fault mechanism (Table 3). In both classes, distinct patterns of the relationship $v_F(M > 5.5) \sim f(b)$ can be observed given the fault mechanism (Fig. 13).

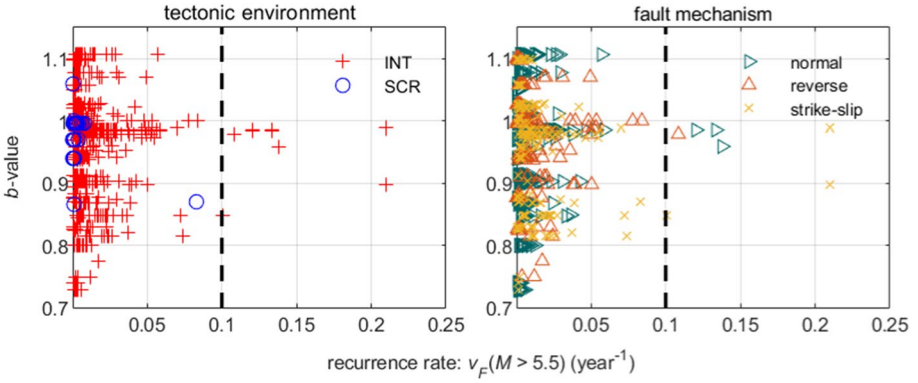

Fig. 12 b-value versus $v_F(M > 5.5)$ per tectonic environment and fault mechanism [the dashed vertical line separates the low from high recurrence rate class]

Table 3 Logic tree formulation for the b-value based on $v_F(M > 5.5)$ classification

Recurrence rate class	Tectonic environment	Fault mechanism
Low	INT, SCR	Normal, reverse, strike-slip
High	INT	Normal, reverse, strike-slip

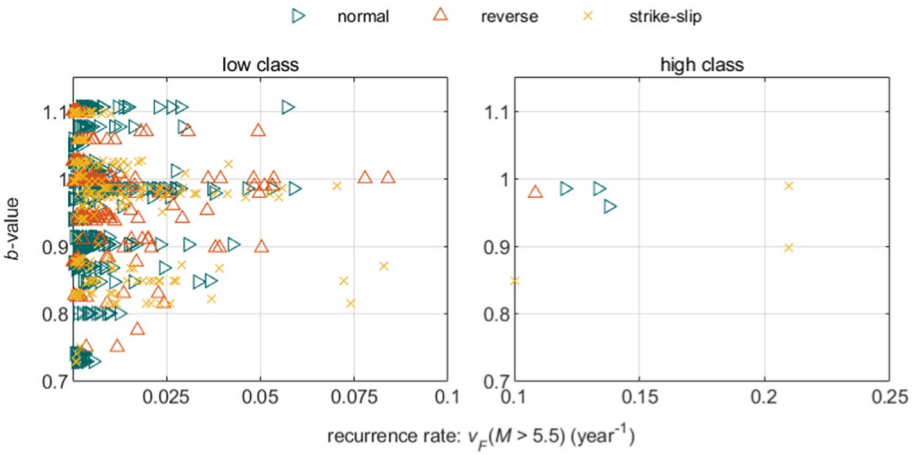

Fig. 13 Gutenberg-Richer b-value from ESHM20 versus $v_F(M > 5.5)$ estimated after Eq. (7) using ESHM20 values; results are shown here per fault mechanism in both recurrence rate classes

The logic tree branches for the b-value were distinguished using the k-means clustering method (Mackay 2005) to near-optimally partition the b-values into discrete sets that minimize the within-cluster sum of squares. The clustering was applied separately for each recurrence rate class as per Table 4. Clustering for INT and SCR faults per fault mechanism for the low recurrence rate class is illustrated in Figs. 14 and 15,

Table 4 Clusters of b-value per recurrence rate [$v_F(M > 5.5)$] class, tectonic environment, and fault mechanism

Recurrence rate class	Tectonic environment	Fault mechanism	C1	C2	C3	C4	C5	C6
Low	INT	Normal	0.7289[†] (0.1050)[‡]	0.8681 (0.1603)	0.9027 (0.2362)	0.9853 (0.2303)	1.0259 (0.1399)	1.1063 (0.1283)
		Reverse	0.8260 (0.0833)	0.8830 (0.1488)	0.9409 (0.2143)	0.9960 (0.2383)	1.0259 (0.1190)	1.0985 (0.1190)
		Strike-slip	0.8297 (0.1830)	0.8770 (0.1404)	0.9544 (0.0681)	0.9784 (0.2383)	1.0259 (0.2298)	1.0971 (0.1404)
	SCR	Normal	0.9397 (0.3030)	0.9700 (0.6667)	1.0592 (0.0303)			
		Reverse	0.9960 (0.8750)	1.0000 (0.1250)				
		Strike-slip	0.8700 (0.1667)	0.9960 (0.8333)				
High	INT	Normal	0.9853 (1.0000)					
		Reverse	0.9784 (1.0000)					
		Strike-slip	0.8734 (0.6667)	0.9891 (0.3333)				

[†]Cluster centroid (logic tree branch value)

[‡]Cluster weight factor (logic tree branch weight factor)

respectively. As expected, a lot of clusters were required for INT faults, contrary to SCR faults. The appropriate clustering of b-values per fault mechanism for the high recurrence rate class is illustrated in Fig. 16. The limited number of faults with a high recurrence rate in the cases of normal and reverse faults drove the k-means algorithm to create a single cluster. Finally, all clusters of b-values (centroid and weight factor) are summarized in Table 4.

3.3.2 Logic tree of maximum earthquake magnitude

The G-R law for estimating the probability of future earthquake magnitudes is bounded between a minimum value of engineering significance and a "physics-based" upper bound value (M_{max}). The latter is a seismogenic parameter that is usually unknown to the engineer/designer, being highly uncertain and typically related to the dimensions of the fault, namely length, width, area (Wells and Coppersmith 1994; Wang 2018). One can explore the M_{max} values of the fault database, similarly to what was done for the b-values. Still, this could lead to multiple clusters of M_{max} given fault length, resulting to a substantial increase in the size of the logic tree and the needed calculations. Instead, it was decided to take advantage of already available models, i.e., obtain the M_{max} values from the fault scaling relations of Leonard (2014) based on the fault length. The empirical expressions of Leonard (2014) relating earthquake magnitude and fault length (mean value and standard

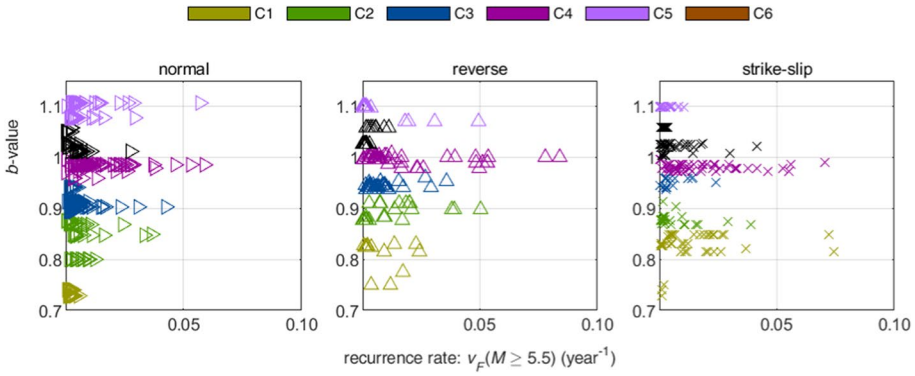

Fig. 14 Clustering of b-values with respect to $v_F(M > 5.5)$: INT faults at low recurrence rate class

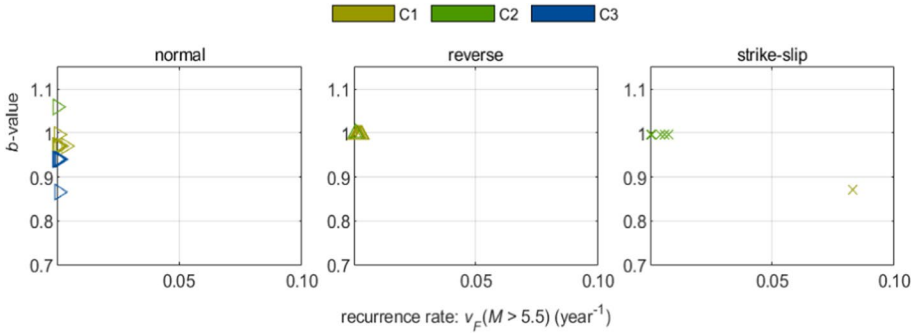

Fig. 15 Clustering of b-values with respect to $v_F(M > 5.5)$: SCR faults at low recurrence rate class

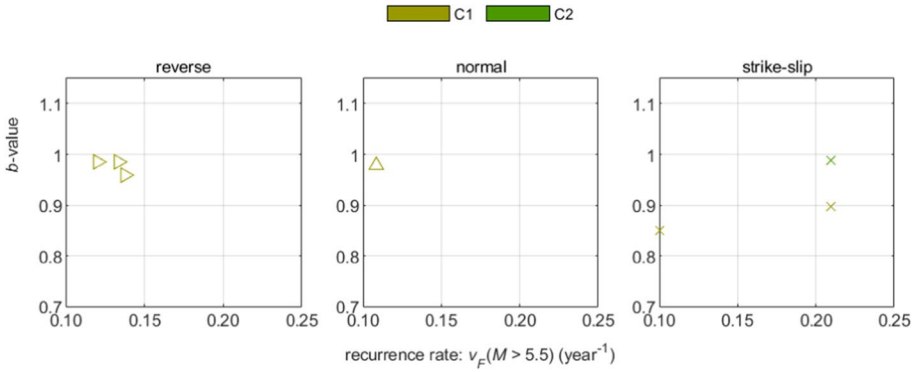

Fig. 16 Clustering of b-values with respect to $v_F(M > 5.5)$: INT faults at high recurrence rate class

deviation) are listed in Table 5. It is noted that the scaling relations of Leonard (2014) were utilized within EFSM20 and ESHM20.

The uncertainty on the estimation of M_{max} was handled through a logic tree formulation per tectonic environment and style-of-faulting. In each case, three branches were considered as per Table 6, where $M_{max,A}$ is the average value, while $M_{max,L}$, $M_{max,U}$ are the

Table 5 Empirical fault scaling relation $M_{max} = a + \beta \log_{10} L_F$ after Leonard (2014)

Tectonic environment	Fault mechanism	a	β	a_{min} †	a_{max} ‡	Range of L_F (km)
INT	Normal	4.24	1.667	3.81	4.73	> 10.0
	Reverse	4.24	1.667	3.81	4.73	> 10.0
	Strike-slip	4.17	1.667	3.87	4.45	3.4–40.0
		5.23	1.000	4.84	5.62	> 40.0
SCR	Normal	4.32	1.667	4.12	4.51	> 10.0
	Reverse	4.32	1.667	4.12	4.51	> 10.0
	Strike-slip	4.25	1.667	4.07	4.43	10.0–60.0
		5.43	1.000	5.25	5.62	> 60.0

The parameter β is a constant and the standard deviation of the relation equals the standard deviation of parameter a

†Mean minus one standard deviation

‡Mean plus one standard deviation

Table 6 Logic tree formulation for M_{max}

Magnitude value	Weight factor
$M_{max,L} = a_{min} + \beta \log_{10} L_F$	$w_L = (1 - w_m)/2$
$M_{max,A} = a + \beta \log_{10} L_F$	$w_A = w_m$
$M_{max,U} = a_{max} + \beta \log_{10} L_F$	$w_U = (1 - w_m)/2$

average minus/plus one standard deviation, respectively. The standard deviation is equal to $(a_{max} - a_{min})/2$, where a_{max} and a_{min} are given in Table 5. The weight factors for each branch are also provided in Table 6, where w_m was computed for each case so as to obtain the same standard deviation provided by Leonard (2014).

At this point it should be noted that the fault slip rate, which can be instrumentally monitored, is considered constant for a particular fault. Therefore, when the maximum earthquake magnitude is modified within a logic tree formulation as per Table 6, the number of events, as expressed via the recurrence rate v_F, has to be adjusted in order to be consistent with the constant slip rate. This is because, for example, an event of high magnitude leads to the release of more energy than a low magnitude one. Thus, a high M_{max} that would allow such high-magnitude events to occur, should be combined with an overall reduced rate events in order for the energy balance to be stable. In other words, the energy released due to earthquakes should balance the energy introduced due to slip. This may be achieved by pairing a high estimate for M_{max} with a low a-value for the G-R law and vice versa. Theoretically, an appropriate formula should be used, as the one proposed by Youngs and Coppersmith (1986), to relate the earthquake magnitude, the slip rate, and the recurrence rate among other parameters. However, the proposed methodology is generic and such a formula cannot be practically implemented because the developed logic tree for M_{max} (Table 6) has to deal with numerous different faults, rather than be optimized for a single one.

To overcome this hurdle and be consistent with the constant slip rate, a generic logic tree is adopted, following the actual trends but correcting via the mean value of many faults. Specifically, the hazard curves calculated with $M_{max,L}$ (low maximum magnitude value) were weighted by the $\text{mean}(a_{GR,ML})/\text{mean}(a_{GR,MA})$ ratio, while the hazard

Table 7 Ratios of mean a-values of the G-R law to account for the constant slip rate, as calculated per given recurrence rate class, tectonic environment, and fault mechanism

Recurrence rate class	Tectonic environment	Fault mechanism	$\text{mean}(a_{GR,ML})/\text{mean}(a_{GR,MA})$	$\text{mean}(a_{GR,MU})/\text{mean}(a_{GR,MA})$
Low	INT	Normal	1.0861	0.9176
		Reverse	1.0716	0.9436
		Strike-slip	1.0769	0.9212
	SCR	Normal	1.1230	0.8167
		Reverse	1.0742	0.9382
		Strike-slip	1.0721	0.9206
High	INT	Normal	1.0313	0.9349
		Reverse	1.0475	0.9501
		Strike-slip	1.0562	0.9410

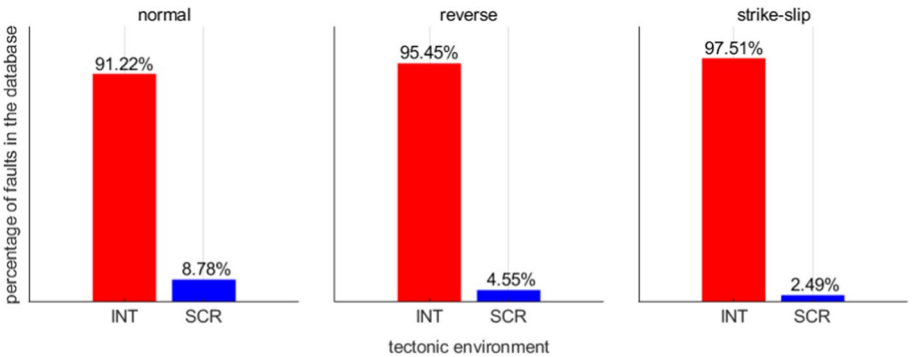

Fig. 17 Percentage of faults with respect to the tectonic environment (INT versus SCR) per mechanism for the low recurrence rate class

curves calculated with $M_{max,U}$ (high maximum magnitude value) were multiplied with $\text{mean}(a_{GR,MU})/\text{mean}(a_{GR,MA})$, where the corresponding means were taken over all faults within a "bin" of given tectonic environment, fault mechanism, and recurrence rate class. For the faults falling within each such bin, $\text{mean}(a_{GR,ML})$ is the mean of pertinent a-values of the G-R law from the fault database that correspond to the low magnitude value, $\text{mean}(a_{GR,MA})$ is the mean of a-values that correspond to the average magnitude value, and $\text{mean}(a_{GR,MU})$ is the mean of a-values that correspond to the high magnitude value. The final ratios are tabulated in Table 7.

3.3.3 Logic tree of tectonic environment

The tectonic environment of the fault should normally be a known property. Yet, it will most probably be an unknown to a practitioner and code user. Thus, it becomes a source of epistemic uncertainty to be handled within a logic tree formulation for the low recurrence rate class, which is the only environment where both INT and SCR faults can coexist. In

the developed single-level logic tree per fault mechanism, the weight factor of each one of the two branches, namely INT and SCR faults, equals the percentage of faults in each tectonic environment, as illustrated in Fig. 17.

3.3.4 Combined 2/3-level logic tree

In total, six logic trees are developed per recurrence rate class and fault mechanism, namely three logic trees (normal, reverse, and strike-slip fault mechanism) in low recurrence rate class and three logic trees (normal, reverse, and strike-slip fault mechanism) in high recurrence rate class. The combined 2/3-level logic tress are presented indicatively for normal fault mechanism at low recurrence rate class in Fig. 18 and at high recurrence rate in Fig. 19. It is recalled that only INT faults can be found in high recurrence rate class (see Sect. 3.3.1, Tables 3, and 4).

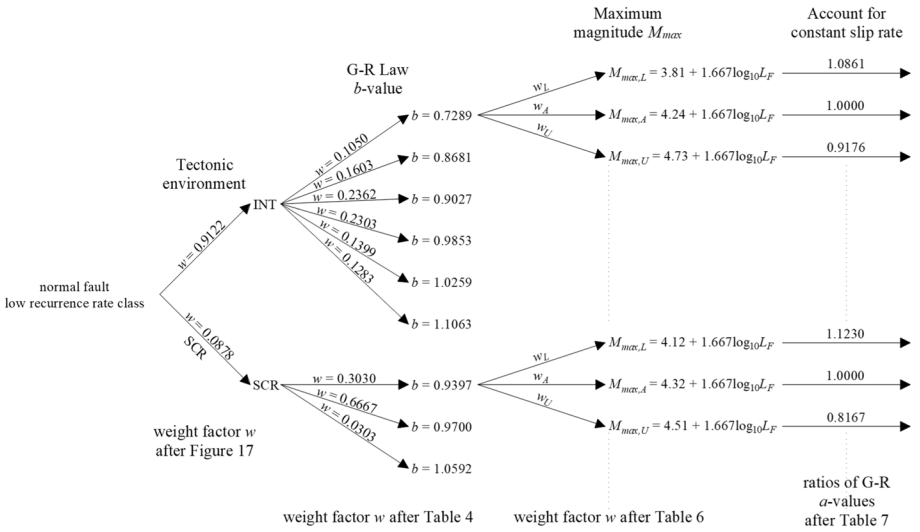

Fig. 18 Logic tree for normal fault at low recurrence rate class

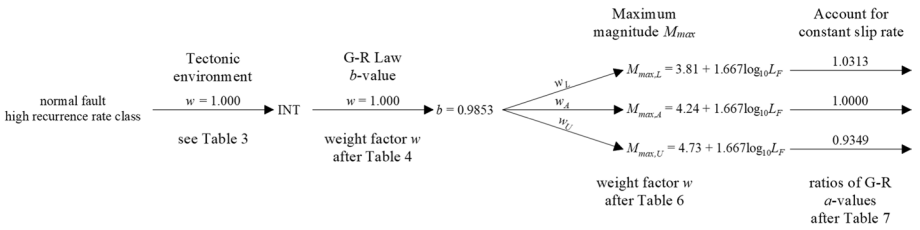

Fig. 19 Logic tree for normal fault at high recurrence rate class

Table 8 Analysis scheme for each PFDHA

Level		
1	Input parameters	Fault length (L_F) and crossing point (X_L)
2		Recurrence rate class: low / high (Table 1)
3		Fault mechanism: normal / reverse / strike-slip
4	Logic tree	Tectonic environment [interplate (INT) / stable continental region (SCR)]: Analysis per recurrence rate class and fault mechanism: INT and SCR faults considered for low recurrence rate class with weight factors after Fig. 17, while only INT faults are considered for high recurrence rate class
5		G-R b-value: Analysis per recurrence rate class, tectonic environment, and fault mechanism with mean values and weight factors after Table 4
6		Maximum earthquake magnitude (M_{max}): Analysis per tectonic environment and fault mechanisms with mean values after Table 5 and corresponding weight factors after Table 6

3.4 PFDHA results

PFDHAs were carried out following the analysis scheme presented in Table 8 for a range of fault lengths $10\,\text{km} \le L_F \le 300\,\text{km}$ and for crossing points $0.10 \le X_L \le 0.50$, the latter with a step of 0.05. The probability of exceedance (PoE) after Eq. (5) was obtained from each analysis.

Polynomial surface fitting was carried out on the results for predefined fault displacement values of Table A1 through Table A3 with respect to fault length and crossing point. The statistical model of Eq. (2) was developed separately for each recurrence rate class and fault mechanism. Indicative results of the fitted surfaces for normal faults at the low and high recurrence rate classes are depicted in Figs. 20 and 21, respectively. The natural logarithm of the fault length ($\ln L_F$) with $10\,\text{km} \le L_F \le 300\,\text{km}$ (see Sect. 3.2) and the crossing point (X_L) with $0 \le X_L \le 0.50$ are shown in the two horizontal axes, while the natural logarithm of the probability of exceedance ($\ln PoE$) obtained after Eq. (5) is shown in the vertical axis. Essentially, the function $f_L\left(\Delta_F, L_F, X_L\right)$ of Eq. (2) is $f_L\left(\Delta_F, L_F, X_L\right) = PoE$. Note that although a sum-of-square-errors criterion was minimized for optimal fitting, this is not a regression, where overfitting and bias-variance considerations are important; instead, it is a curve-fitting operation, where there is only one valid outcome for every combination of inputs and ease of use is our only limitation in terms of the fitted form.

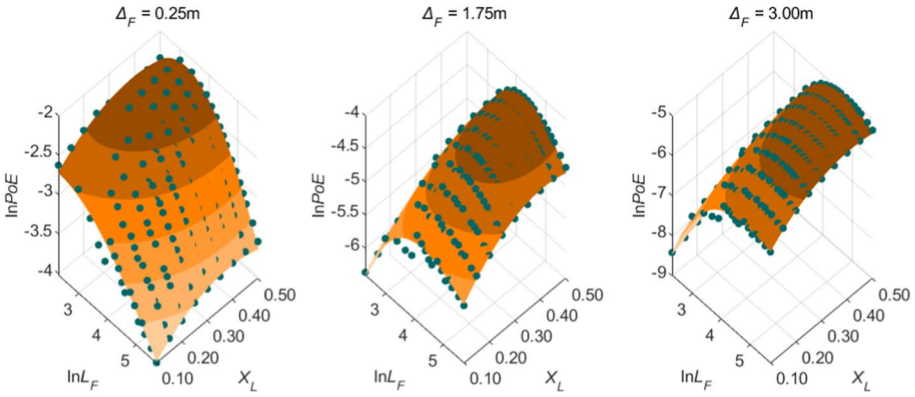

Fig. 20 Surface fitting for normal fault, low recurrence rate class, and various fault displacements (fault length L_F in km)

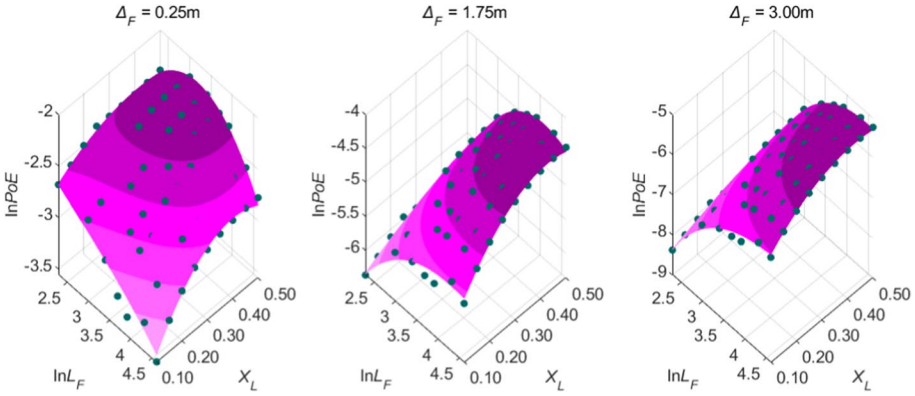

Fig. 21 Surface fitting for normal fault, high recurrence rate class, and various fault displacements (fault length L_F in km)

4 Methodology evaluation and application

4.1 Evaluation of results

The proposed methodology (abbreviated as the EN1998-4 approach) is applied to an indicative set of faults from the fault database (see Sect. 3.2), featuring different dimensions and seismological properties. The INT faults under examination are listed in Table 9 and the SCR faults in Table 10. The EN1998-4 approach is evaluated by comparing the obtained return period after Eq. (1) for the predefined fault displacement values of Table A1 through Table A3 to the one obtained from a full PFDHA after Eq. (4). It is noted that the maximum earthquake magnitude considered in a fault displacement hazard analysis affects significantly the resulting MAFs (Melissianos et al. 2023) or equivalently the return period. Thus, it is important to examine this effect when comparing the EN1998-4 approach with a

Table 9 Interplate (INT) faults under examination

Fault name	Tectonic environment	Fault mechanism	L_F(km)	$M_{0.02}$	$M_{0.05}$	M_{avg}	$M_{0.95}$	$M_{0.98}$	M_{L2014}
ALCF009	INT	Normal	30.00	6.50	6.60	6.80	7.10	7.20	6.70
BGCF00V	INT	Normal	29.92	6.10	6.20	6.40	6.70	6.80	6.70
ITCF03K	INT	Normal	30.06	6.60	6.60	6.80	7.10	7.20	6.70
FRCF00F	INT	Reverse	159.83	6.40	6.50	6.70	7.00	7.10	7.91
HRCF005	INT	Reverse	159.91	6.90	7.00	7.20	7.50	7.60	7.91
ITCF002	INT	Reverse	160.18	6.20	6.20	6.50	6.80	6.90	7.91
GECF00F	INT	Strike-slip	49.68	6.80	6.90	7.10	7.40	7.50	6.93
HRCF00I	INT	Strike-slip	49.92	6.40	6.40	6.70	7.00	7.10	6.93
TRCF02H	INT	Strike-slip	49.99	6.40	6.40	6.70	7.00	7.10	6.93

Table 10 Stable continental region (SCR) faults under examination

Fault name	Tectonic environment	Fault mechanism	L_F(km)	$M_{0.02}$	$M_{0.05}$	M_{avg}	$M_{0.95}$	$M_{0.98}$	M_{L2014}
PTCF00Y	SCR	Normal	38.93	6.90	6.90	7.20	7.50	7.60	6.91
PTCF019	SCR	Normal	35.59	6.70	6.80	7.00	7.30	7.40	6.91
ESCF025	SCR	Strike-slip	17.81	6.40	6.40	6.90	6.90	7.00	6.41
ESCF02C	SCR	Strike-slip	17.84	6.40	6.40	6.60	6.90	7.00	6.41

full PFDHA. For the latter case, five values of M_{max}, obtained from the fault database, were considered for each fault: $M_{0.02}$ is the 2% value, $M_{0.05}$ is the 5% value, M_{avg} is the average value, $M_{0.95}$ is the 95% value, and $M_{0.98}$ is the 98% value.

The results for the INT faults are presented in Fig. 22 and for SCR in Fig. 23. It is observed that the EN1998-4 approach is conservative in general, leading to lower return periods than a full PFDHA. It is recalled that the maximum earthquake magnitude considered in the development of the EN1998-4 approach was calculated using the empirical fault scaling relations of Leonard (2014); the mean estimated magnitude is shown in Table 9 and Table 10 as M_{L2014} for comparison reasons. In the case where the M_{L2014} value is close to the lower percentiles of the magnitude values from the database, then the return periods obtained from the EN1998-4 approach are quite higher than the ones obtained from PFHDA, e.g., see the ITCF03K, GECF00F, PTCF00Y, and ESCF02C faults. These form the bulk of the rare cases where the EN1998-4 approach would end up being unconservative.

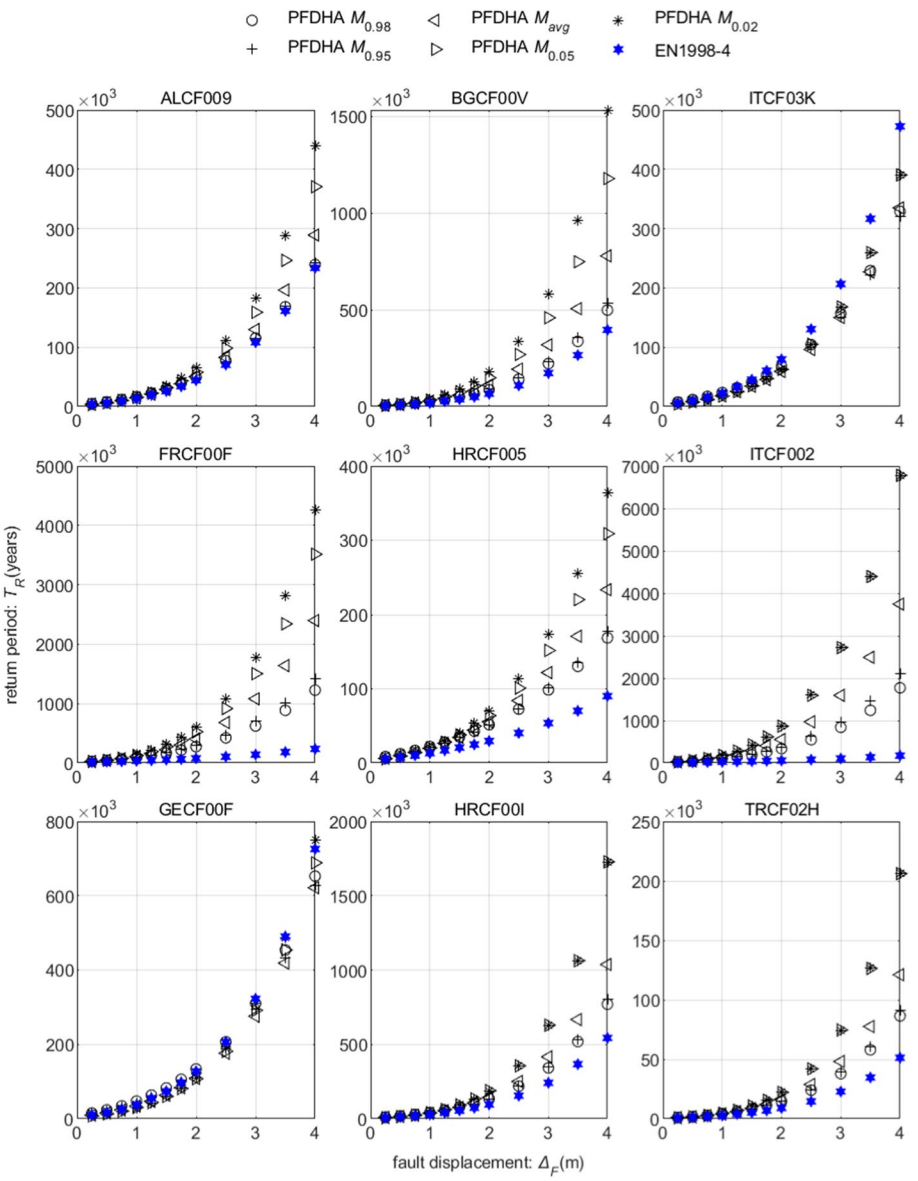

Fig. 22 INT faults: comparison of return periods for predefined fault displacement values between the EN1998-4 approach and PFDHA (5 different maximum earthquake magnitude values considered)

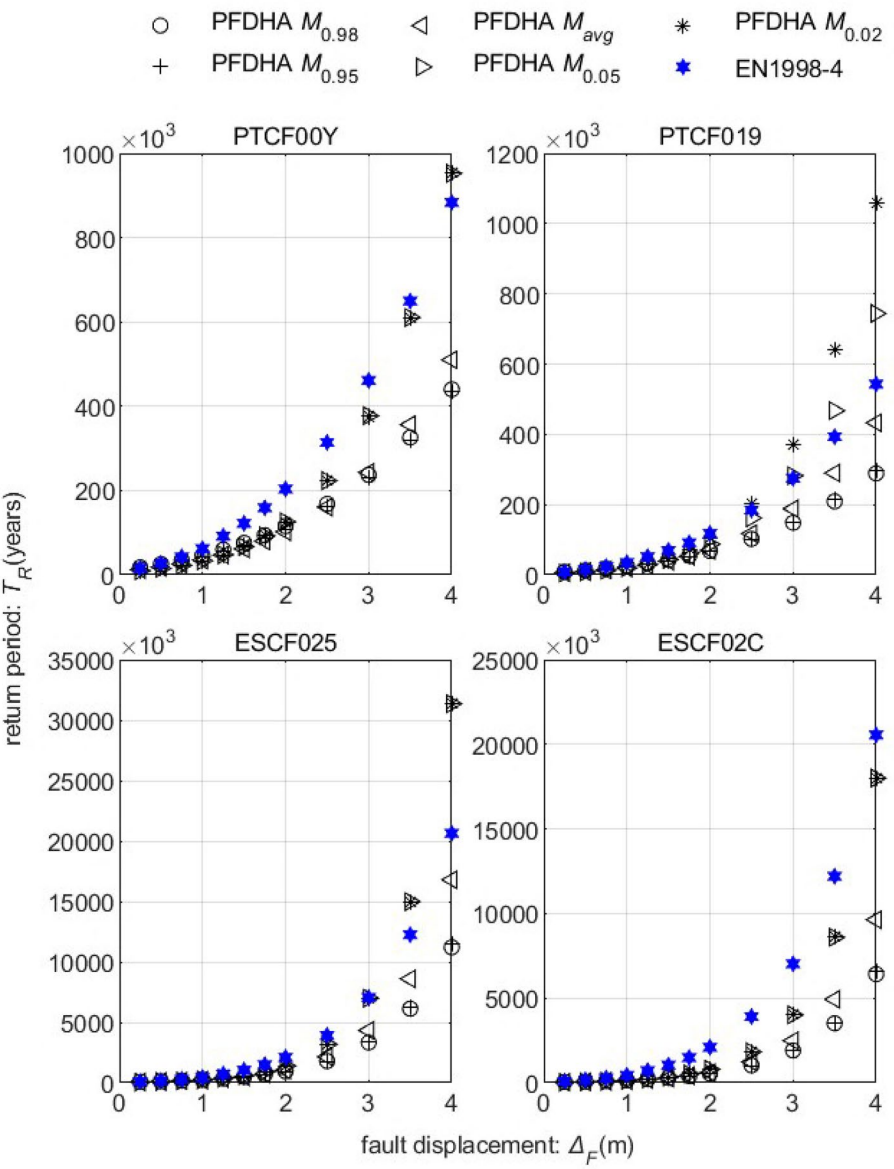

Fig. 23 SCR faults: comparison of return periods for predefined fault displacement values between the EN1998-4 approach and PFDHA (5 different maximum earthquake magnitude values considered)

Table 11 Case study faults

Area	Fault name	Tectonic environment	Fault mechanism	L_F(km)	ν_F(year^{-1})	Recurrence rate class
France–Spain border						
Pyrenees	FRCF00W	INT	Normal	82.39	0.0002	Low
	ESCF01Y	INT	Normal	76.63	0.0004	Low
	ESCF00P	INT	Normal	26.77	0.0005	Low
France						
Northwest	FRCF00V	SCR	Reverse	159.74	0.0008	Low
	FRCF00P	SCR	Normal	36.14	0.0001	Low
	FRCF00S	SCR	Normal	215.71	0.0013	Low
Germany						
Aachen	DECF005	INT	Normal	54.51	0.0009	Low
	DECF007	INT	Normal	21.81	0.0001	Low
Frankfurt	DECF000	INT	Normal	165.70	0.0031	Low
Austria						
Wien	ATCF004	INT	Normal	54.73	0.0019	Low
	ATCF005	INT	Strike-slip	156.25	0.0023	Low
	ATCF008	INT	Strike-slip	116.11	0.0008	Low
	ATCF00A	INT	Strike-slip	103.86	0.0068	Low
Portugal						
Central and North	PTCF010	SCR	Strike-slip	221.16	0.0077	Low
	PTCF013	SCR	Reverse	130.37	0.0033	Low
	PTCF014	SCR	Reverse	161.20	0.0028	Low
	PTCF018	SCR	Normal	12.41	0.0007	Low
Slovenia						
Ljubljana	SICF00A	INT	Strike-slip	13.51	0.0001	Low
	SICF00K	INT	Reverse	16.35	0.0008	Low
	SICF00J	INT	Strike-slip	75.12	0.0049	Low
West	SICF004	INT	Strike-slip	74.94	0.0046	Low
Bulgaria						
Northeast	BGCF011	INT	Normal	89.84	0.0010	Low
	BGCF015	INT	Normal	177.37	0.0014	Low
Sofia	BGCF00O	INT	Normal	70.28	0.0028	Low
	BGCF00P	INT	Normal	50.04	0.0036	Low
Italy						
Calabria region	ITCF03N	INT	Normal	65.21	0.0098	Low
	ITCF03Q	INT	Normal	44.76	0.0047	Low
	ITCF03I	INT	Strike-slip	40.14	0.0021	Low
Attica region						
Attica region	GRCF04N	INT	Normal	40.15	0.0149	Low
	GRCF014	INT	Normal	59.70	0.0074	Low
	GRCF020	INT	Normal	14.96	0.0016	Low
	GRCF01I	INT	Normal	32.04	0.0030	Low
Turkey						
Northwest	TRCF00D	INT	Strike-slip	65.68	0.0234	Low
	TRCF00G	INT	Normal	78.90	0.0365	Low
	TRCF049	INT	Strike-slip	29.92	0.0295	Low

Table 12 Empirical estimates of $\Delta_{L2014} \sim f(L_F)$ after Leonard (2014)

Tectonic environment	Expression for median value (Δ_{L2014} in m, L_F in km)	Expression parameters (α/β) per fault mechanism		
		Normal	Reverse	Strike-slip
INT	$\log_{10}(\Delta_{sub}) = \alpha + \beta \log_{10}(1000 L_F)$ $\Delta_{L2014} = \Delta_{sub}/1.32$	− 3.799/0.833	− 3.799/0.833	$10 \le L_F \le 40$ − 3.844 /0.833 $L_F > 40$ − 2.310/0.500
SCR	$\log_{10}(\Delta_{sub}) = \alpha + b \log_{10}(1000 L_F)$ $\Delta_{L2014} = \Delta_{sub}/1.32$	− 3.572/0.833	− 3.572/0.833	$10 \le L_F \le 60$ − 3.615/0.833 $L_F > 60$ -2.022 / 0.500

4.2 Case studies

The fault displacement using the EN1998-4 approach was calculated for design return periods of 2500 years ($\Delta_{F,2500}$) and 5000 years ($\Delta_{F,5000}$) for a set of indicative faults in Europe (Table 11) that are located close to industrial areas, large cities, and important infrastructure. It is noted that the 2500 years and 5000 years return periods correspond to the Near Collapse limit state for consequences classes CC3-a and CC3-b, respectively, as dictated by prEN 1998-4:2022 (European Committee for Standardisation 2022). The crossing was assumed to be located at the middle of the fault ($X_L = 0.50$). Additionally, the median estimate of fault displacement by Leonard (2014) after Table 12 are presented for comparison reasons. The aim is to showcase the difference on the obtained fault displacement values between the hazard-consistent EN1998-4 approach and a "seismicity-agnostic" deterministic one, where only the fault dimensions are taken into account. Note that the latter approach disregards the fault seismicity and the magnitude that would correspond to a given return period for each fault (Davis 2008), representing an engineering-level approximation of low fidelity.

The case study faults are examined by country in Fig. 24 through Fig. 26.

Pyrenees: Three indicative faults in the Pyrenees at the France–Spain border were examined. It is observed that due to the significantly low recurrence rate (lower than 0.0005 events on average per year with magnitude $M \ge 5.5$), the resulting displacement values for both return periods are set equal to the minimum, namely $\Delta_F = 0.10$ m (Fig. 24).

France: The tectonic environment in the northwest part of France is SCR. The recurrence rate is quite low and, consequently, the resulting fault displacements are set equal to the minimum value ($\Delta_F = 0.10$ m) [Fig. 24].

Germany: Three normal faults were selected as a case study in Germany, one in the greater area of Aachen and the other around Frankfurt. In all cases the resulting fault displacements from the EN1998-4 approach are equal to the minimum value ($\Delta_F = 0.10$ m), while the obtained values from the empirical fault scaling relations are high, especially for the very long DRCF000 fault with $L_F = 165.70$ km) [Fig. 24].

Austria: INT strike-slip and normal faults are located around Wien. The evaluation of analysis results indicates that the recurrence rate is the critical parameter driving the resulting fault displacements (Fig. 25).

Portugal: In the central and north parts of Portugal there are SCR faults with all three mechanisms. They have in general low recurrence rates, leading to low fault displacement values, while the Δ_{L2014} values are considerably high due to the large length (Fig. 25).

Slovenia: Numerous faults are located in the northwest part of the Balkan Peninsula in Slovenia. Four indicative INT faults were selected and examined. One should notice the SICF004 and SICF00J strike-slip faults with a higher recurrence rate, compared to the others. The resulting fault displacement values for these faults are roughly equal to $\Delta_F = 0.50\,\text{m}$ (Fig. 25).

Bulgaria: INT normal faults with various lengths and recurrence rates have been selected in the northeast part of Bulgaria and around the capital Sofia (Fig. 26).

Italy: In the industrial area of Calabria in Italy (south part) there are INT faults with considerable recurrence rates and consequently very high fault displacements, as obtained from the EN1998-4 approach (Fig. 26).

Greece: In the Attica region and in particular north, west, northwest of Athens, there are INT normal faults with relatively short length but high recurrence rates. The obtained fault displacement values are very high, indicating a non-negligible threat for potential crossing lifelines (Fig. 26).

Turkey: The North Anatolian fault system in Turkey is a well-known and studied active seismic area. Three indicative normal and strike-slip faults located at the south of Marmara Sea were selected and studied. Regardless of the length, the considerably high recurrence rates lead to very high design values for the fault displacement for both return periods. Contrarily, the displacement values derived from the empirical fault scaling relations are low (Fig. 26).

In all cases, the main observation is that the recurrence rate is a dominant parameter that clearly differentiates the resulting displacements for faults of similar length. On the other hand, the "seismicity-agnostic" deterministic approach that neglects the rate and only focuses on the dimensions and mechanism of the fault is bound to be overly conservative in low-recurrence-rate cases (e.g., cases examined in France and Portugal), while unconservative in cases of high recurrence rates (e.g., cases examined in Greece and Turkey).

5 Recurrence rates approximation

The earthquake recurrence rate of an active fault is a critical aspect of the hazard calculations and, in fact, is an external multiplier in Eq. (4), which is typically estimated by earth science experts, i.e., geologists, geophysicists, seismologists, etc. In the absence of such information, the correlation between the recurrence rate and the resulting ground shaking level in the vicinity of the fault can be used. It is preferable to employ engineering-level quantities that are already available in the relevant design code to accomplish this. Herein, we employ the fault length and a seismic design parameter, i.e., $S_{\beta,475}$ estimated at the location of the fault, which is the reference spectral acceleration at period $T_\beta = 1\,\text{s}$ corresponding to a return period of $T_R = 475$ years. This is considered superior to the short period reference acceleration, $S_{\alpha,475}$, as longer periods are better indicators of large magnitude seismicity that is of interest for fault displacements. Seismic hazard maps of the mean and median $S_{\beta,475}$ values are provided in EN1998-1-1:2021 (European Committee for Standardisation 2021) based on the ESHM20 (Danciu et al. 2021). It is acknowledged that even on top of a fault, $S_{\beta,475}$ values may incorporate contributions

Fig. 24 Fault displacements obtained from the EN1998-4 approach for return periods of 2500 years ($\Delta_{F,2500}$) and 5000 years ($\Delta_{F,5000}$), compared against the "seismicity-agnostic" estimate (Δ_{L2014}): Pyrenees, France, and Germany

from all nearby faults and will be sensitive to ground motion models. Still, it can be conservatively assumed that the underlying fault under consideration contributes the most, indicating a strong positive correlation of $S_{\beta,475}$ with v_F. $S_{\beta,475}$ values on each fault trace of the database were obtained through appropriate interpolation on the $S_{\beta,475}$ seismic hazard maps. To avoid any over-representation of locations, multiple $S_{\beta,475}$ values were computed along each fault trace, and their average was taken as representative of the entire fault. Such averaged values are derived for both the mean and the median $S_{\beta,475}$, and plotted versus v_F in Figs. 27 and 28, respectively. No clear pattern emerges per tectonic environment or fault mechanism in either case. It was thus decided to build a regression model by considering all faults together.

Equation (8) is the fitted polynomial expression of the model (Fig. 29) for the approximated recurrence rate ($v_{F,approx}$). The model metrics are $R^2 = 0.7333$ and standard error $\sigma_{\varepsilon,mean} = 0.7539$ when considering the mean acceleration $S_{\beta,475}$, versus $R^2 = 0.7097$ and $\sigma_{\varepsilon,50} = 0.7867$ when considering the median acceleration $S_{\beta,475}$, indicating a fair but imperfect fit.

$$\ln v_{F,approx} = p_1 + p_2 S_{\beta,475} + p_3 {S_{\beta,475}}^2 + p_4 S_{\beta,475} \ln L_F + p_5 \left(\ln L_F\right)^2 + p_6 {S_{\beta,475}}^3 + p_7 S_{\beta,475} \left(\ln L_F\right)^2 \tag{8}$$

The model of Eq. (8) can be rewritten in a more straightforward form:

$$v_{F,approx} = \exp\left[\begin{array}{l} p_1 + p_2 S_{\beta,475} + p_3 {S_{\beta,475}}^2 + p_4 S_{\beta,475} \ln L_F + \\ p_5 \left(\ln L_F\right)^2 + p_6 {S_{\beta,475}}^3 + p_7 S_{\beta,475} \left(\ln L_F\right)^2 \end{array}\right] \tag{9}$$

ln(•) is the natural logarithm of its argument and the coefficients p_1, p_2,…, p_7 are listed in Table 13 for L_F in km and $S_{\beta,475}$ in units of g.

The regression residuals are estimated as

$$\varepsilon = \frac{\ln v_F - \ln v_{F,approx}}{\sigma_\varepsilon} \tag{10}$$

Negative residuals ($\varepsilon < 0$) reflect an overestimation of the recurrence rate, which is considered to be acceptable conservatism within the framework of a design code. Contrarily, the underestimation ($\varepsilon > 0$) requires some treatment. It is noted here that the aim is not to build an unbiased probabilistic model, but rather a conservative one, suitable for preliminary design.

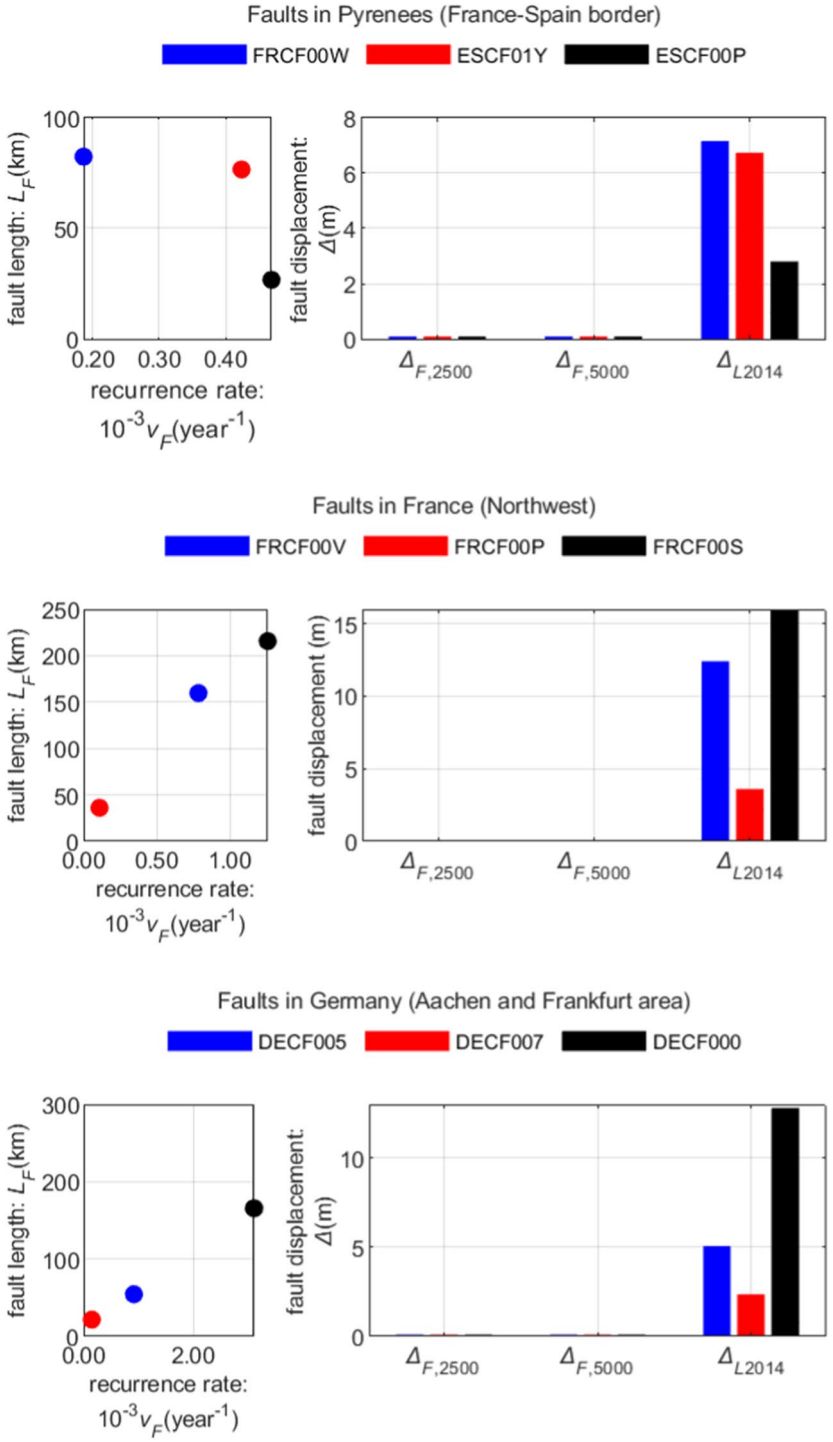
Faults in Pyrenees (France-Spain border)
FRCF00W
ESCF01Y
ESCF00P
fault length: L_F(km)
100
50
0
0.20
0.30
0.40
recurrence rate:
$10^{-3}\nu_F$(year^{-1})
fault displacement: Δ(m)
8
6
4
2
0
$\Delta_{F,2500}$
$\Delta_{F,5000}$
Δ_{L2014}
Faults in France (Northwest)
FRCF00V
FRCF00P
FRCF00S
fault length: L_F(km)
250
200
150
100
50
0
0.00
0.50
1.00
recurrence rate:
$10^{-3}\nu_F$(year^{-1})
fault displacement (m)
15
10
5
0
$\Delta_{F,2500}$
$\Delta_{F,5000}$
Δ_{L2014}
Faults in Germany (Aachen and Frankfurt area)
DECF005
DECF007
DECF000
fault length: L_F(km)
300
200
100
0
0.00
2.00
recurrence rate:
$10^{-3}\nu_F$(year^{-1})
fault displacement: Δ(m)
10
5
0
$\Delta_{F,2500}$
$\Delta_{F,5000}$
Δ_{L2014}

Fig. 25 Fault displacements from the EN1998-4 approach for return periods of 2500 years ($\Delta_{F,2500}$) and 5000 years ($\Delta_{F,5000}$), compared against the "seismicity-agnostic" estimate (Δ_{L2014}): Austria, Portugal, and Slovenia ▶

The regression residuals (ε) versus the actual recurrence rate (ν_F) are illustrated in Fig. 30 along with the 5%, 16%, 50%, 84%, and 95% running quantiles (Haver and Winterstein 2009), employing a symmetric-neighbor window length of 20% of the sample. This is the traditional approach of inspecting a regression model, and it points to a less-than-optimal fit without homoscedastic residuals, indicating unconservative estimates at high actual rates. However, when looking to determine an appropriate confidence factor for correcting (conservatively biasing) the regression model output, the actual rates are not useful; they are not available to the user. Only the approximated rate, $\nu_{F,approx}$, can be employed.

Figure 31 offers this view, showing the residuals against $\nu_{F,approx}$. Attempting to envelop the underestimation area, a multiplicative confidence factor C_F is employed to update/increase $\nu_{F,approx}$, introducing the needed conservative bias:

$$\nu_{F,approx,u} = C_F \nu_{F,approx} \tag{11}$$

Based on Fig. 31, a constant confidence factor $C_F > 1.00$ is considered for $\ln\nu_{F,approx} \leq -3$ with a linear (in log–log space) ramp-down to 1.00 within $-3 \leq \ln\nu_{F,approx} \leq -1$ (see Fig. 32):

$$C_F = \begin{cases} \exp(a_{CF}) & \ln\nu_{F,approx} < -3 \\ \exp\left[a_{CF} - a_{CF}(\ln\nu_{F,approx} + 3)/2\right] & -3 \leq \ln\nu_{F,approx} \leq -1 \\ 1.00 & -1 < \ln\nu_{F,approx} \end{cases} \tag{12}$$

where $\nu_{F,approx}$ is in units of year^{-1}, $a_{CF} = 1.2975 \times \sigma_{\varepsilon,mean} \approx 0.98$ for the mean $S_{\beta,475}$, and $a_{CF} = 1.3323 \times \sigma_{\varepsilon,50} \approx 1.05$ for the median $S_{\beta,475}$. Note that the multiplier of the standard error is chosen as the residual value roughly conforming to the near-constant value of the 95% quantile for low recurrence rates in Fig. 31. It is noted that the quantiles should normally come closer to zero for high rates, yet the large window length of 20% employed in the running quantile scheme is influenced by nearby values and maintains higher absolute values even in the high-rate region.

The recurrence rate values from the database and the (uncorrected/non-updated) approximated ones via Eq. (9) are compared in Fig. 33 for both estimates using the mean and the median acceleration $S_{\beta,475}$. A roughly 50% of underestimation is detected for both cases, namely 50% of values are below the dashed line, indicating that the actual recurrence rate of the faults is higher than the approximated one. Then, the effect of the confidence factor on the approximated recurrence rate is illustrated in Fig. 34, where the recurrence rate values from the fault database are plotted versus the updated approximated values after Eq. (11). The introduction of the confidence factor drives about 40% more values above the dashed line, yielding a coverage ($\nu_{F,approx,u} > \nu_F$) above 90%.

A set of indicative faults with essentially different length and seismological properties is selected from Table 9 and Table 10 to evaluate the results of the recurrence rate

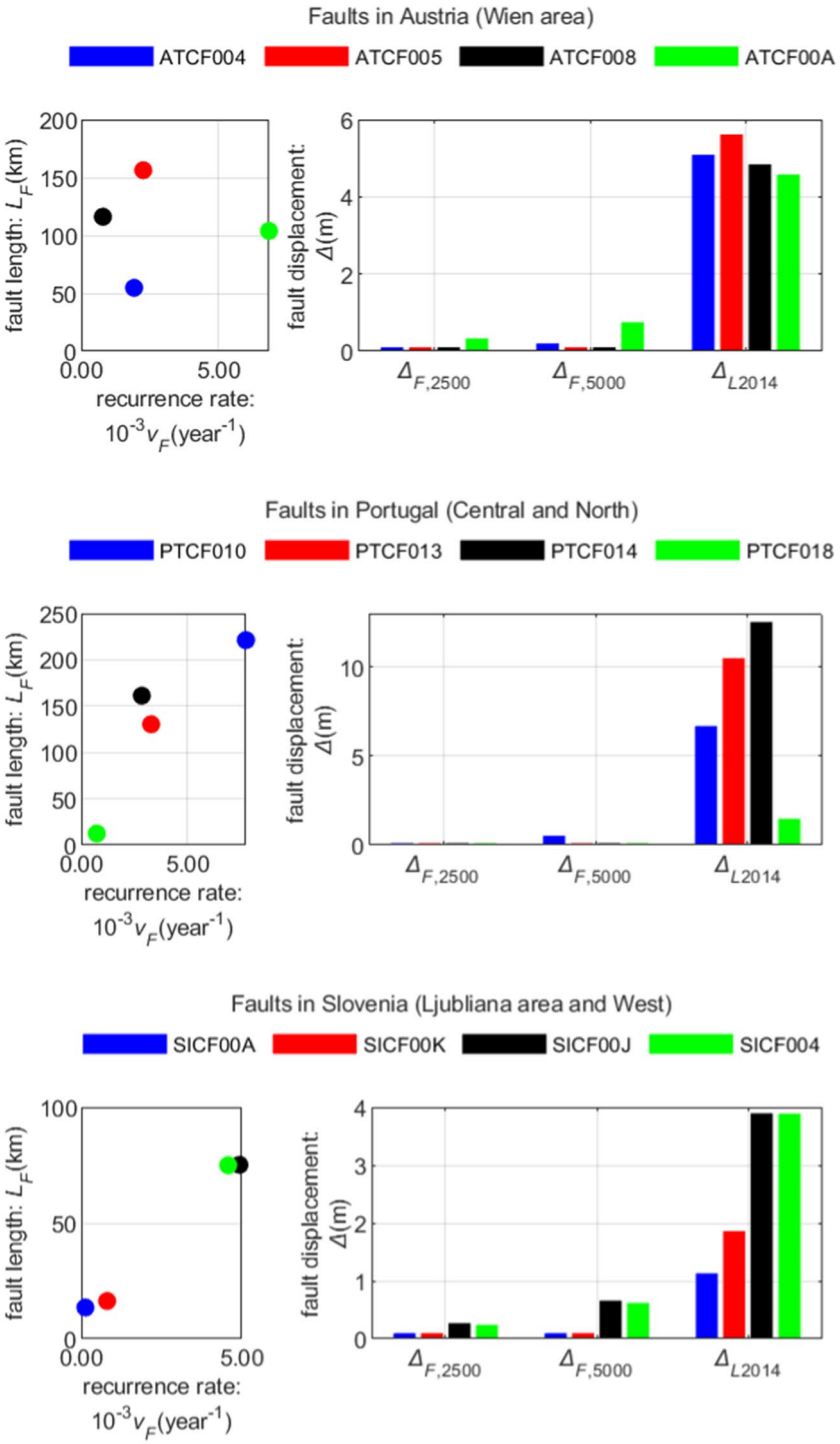
Faults in Austria (Wien area)
ATCF004
ATCF005
ATCF008
ATCF00A
fault length: L_F(km)
200
150
100
50
0
0.00
5.00
recurrence rate:
$10^{-3}\nu_F$(year^{-1})
fault displacement: Δ(m)
6
4
2
0
$\Delta_{F,2500}$
$\Delta_{F,5000}$
Δ_{L2014}
Faults in Portugal (Central and North)
PTCF010
PTCF013
PTCF014
PTCF018
fault length: L_F(km)
250
200
150
100
50
0
0.00
5.00
recurrence rate:
$10^{-3}\nu_F$(year^{-1})
fault displacement: Δ(m)
10
5
0
$\Delta_{F,2500}$
$\Delta_{F,5000}$
Δ_{L2014}
Faults in Slovenia (Ljubliana area and West)
SICF00A
SICF00K
SICF00J
SICF004
fault length: L_F(km)
100
50
0
0.00
5.00
recurrence rate:
$10^{-3}\nu_F$(year^{-1})
fault displacement: Δ(m)
4
3
2
1
0
$\Delta_{F,2500}$
$\Delta_{F,5000}$
Δ_{L2014}

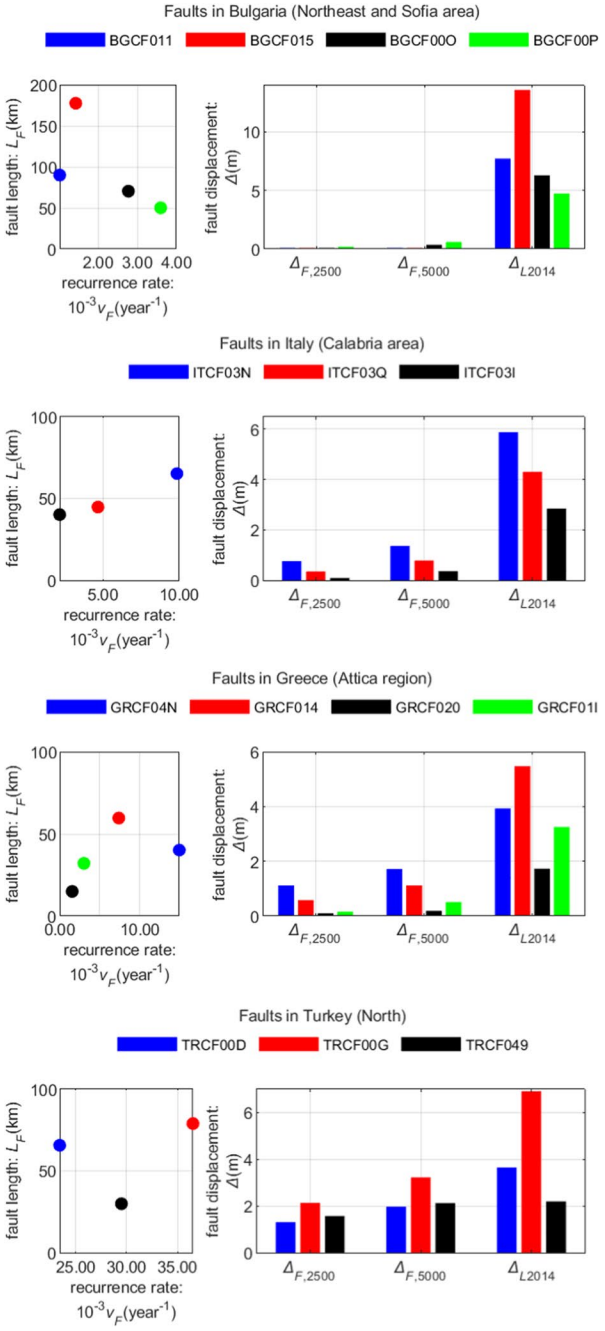

Fig. 26 Fault displacements obtained from the EN1998-4 approach for return periods of 2500 years ($\Delta_{F,2500}$) and 5000 years ($\Delta_{F,5000}$), compared against the "seismicity-agnostic" estimate (Δ_{L2014}): Bulgaria, Italy, Greece, and Turkey

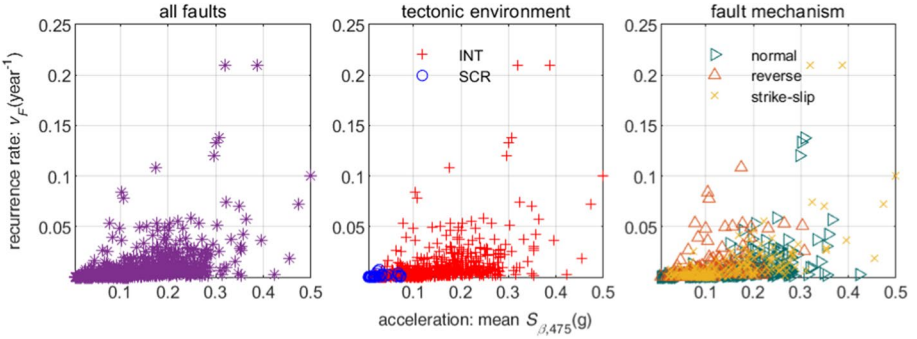

Fig. 27 Earthquake recurrence rate, $v_F(M > 5.5)$ in year^{-1}, database versus mean $S_{\beta,475}$ per tectonic environment and fault mechanism

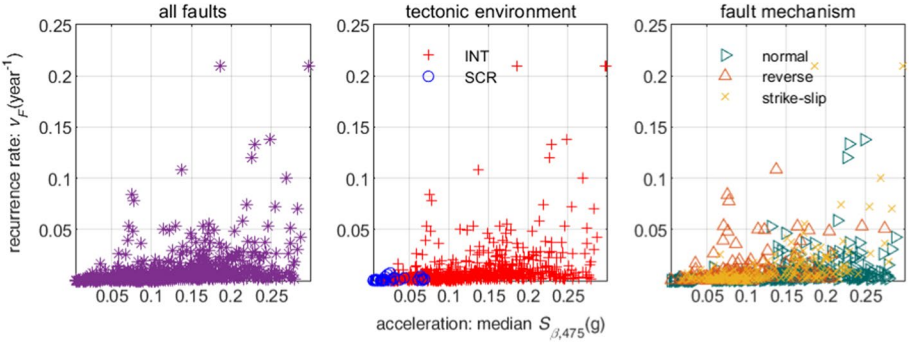

Fig. 28 Earthquake recurrence rate, $v_F(M > 5.5)$ in year^{-1}, versus median $S_{\beta,475}$ per tectonic environment and fault mechanism

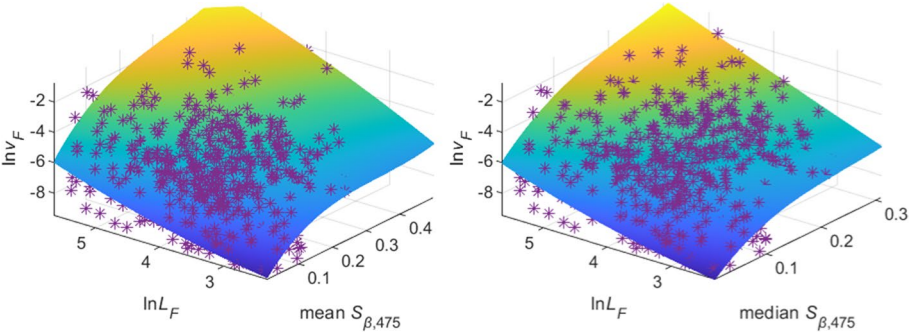

Fig. 29 Surface fitting for v_F versus $S_{\beta,475}$ and fault length (v_F in year^{-1}, $S_{\beta,475}$ in g, L_F in km)

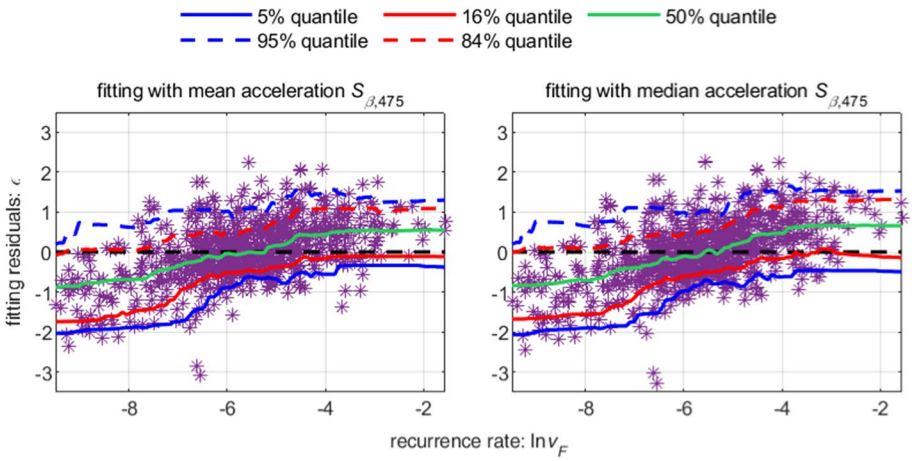

Fig. 30 Regression residuals (ε) versus the actual recurrence rate, v_F (in year^{-1})

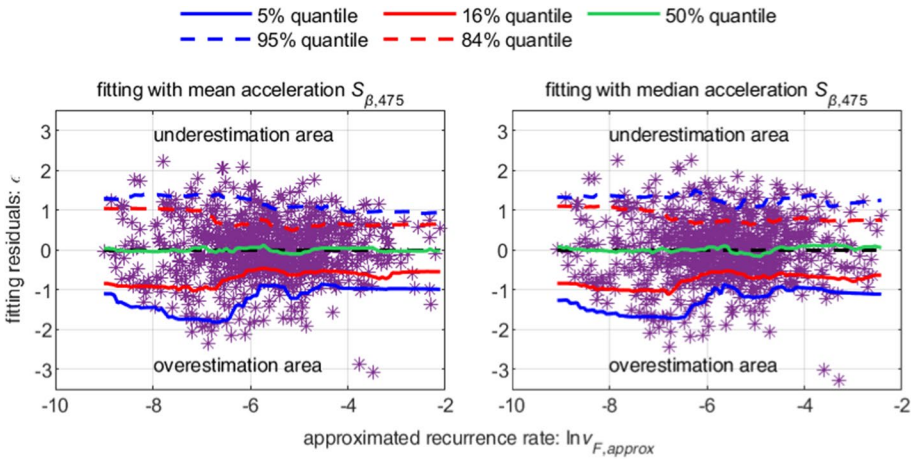

Fig. 31 Fitting residuals (ε) of the statistical model versus the approximated recurrence rate, $v_{F,approx}$ (in year^{-1})

Table 13 Coefficients for estimating the approximated recurrence rate ($v_{F,approx}$) after Eq. (9), derived for L_F in km and $S_{\beta,475}$ in g

Mean $S_{\beta,475}$		Median $S_{\beta,475}$	
Coeff	Value	Coeff	Value
p_1	− 10.1539	p_1	− 10.2940
p_2	16.7322	p_2	23.6696
p_3	− 76.0447	p_3	− 120.9933
p_4	5.4398	p_4	5.0275
p_5	0.1262	p_5	0.1280
p_6	74.1251	p_6	162.7411
p_7	− 0.5065	p_7	− 0.4092

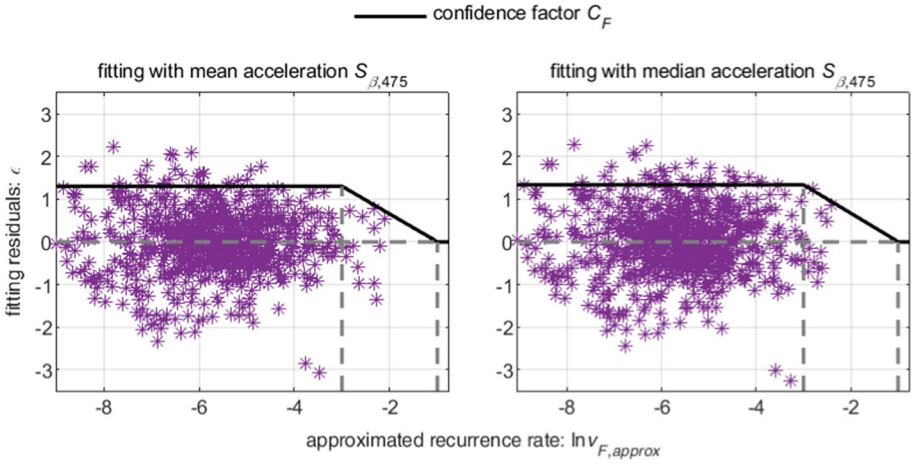

Fig. 32 Confidence factor (C_F) for the approximated recurrence rate $v_{F,approx}$ (in year^{-1})

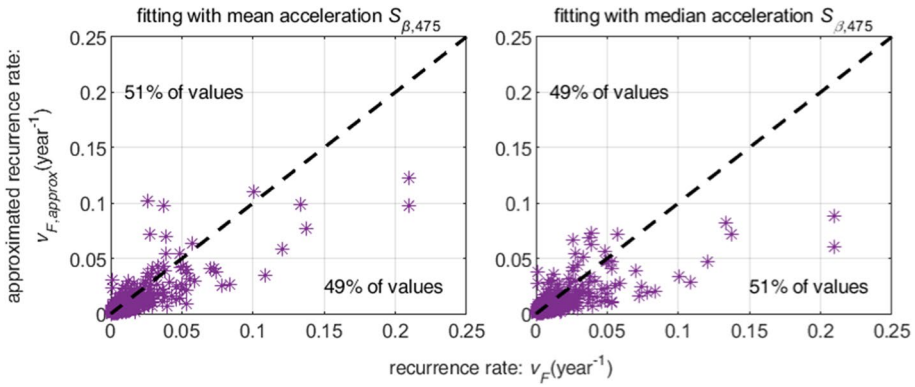

Fig. 33 Comparison of actual recurrence rates (v_F) versus the approximated ones ($v_{F,approx}$)

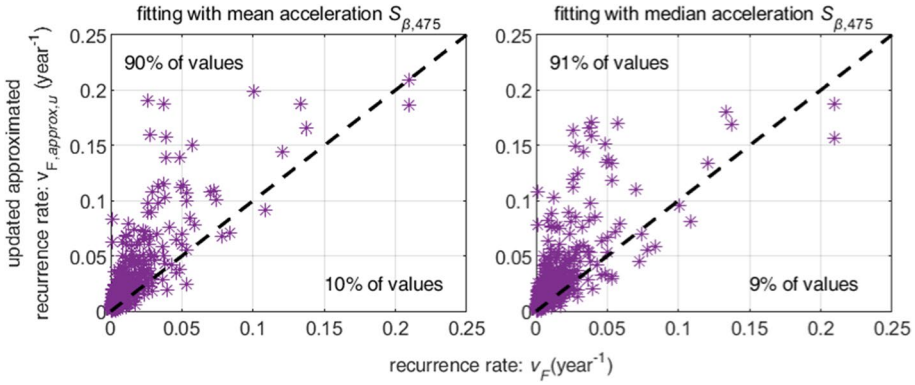

Fig. 34 Comparison of actual recurrence rates (v_F) versus the updated approximated ones ($v_{F,approx,u}$)

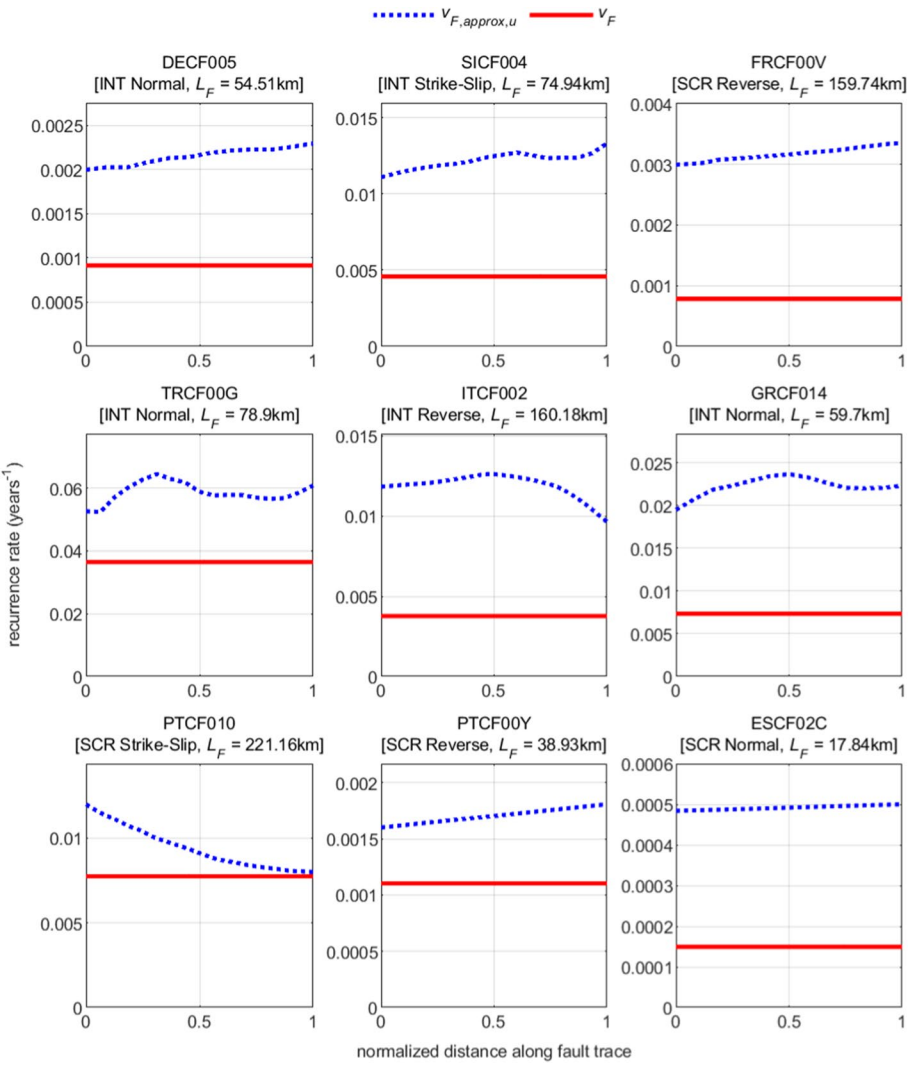

Fig. 35 Comparison of the actual recurrence rate (v_F) versus the updated approximated ones ($v_{F,approx,u}$) calculated at different points along the fault using the mean $S_{\beta,475}$; the distance is measured according to the fault trace node sequence, which is ordered following the right-hand rule (Aki and Richards 1980)

approximation. The mean acceleration $S_{\beta,475}$ is computed via interpolation from the seismic hazard map for several locations on the mapped fault trace. At each location, the updated approximated rate ($v_{F,approx,u}$) is calculated via Eqs. (9), (11), and (12) and is plotted in Fig. 35 with dots. As expected, the rate is changing along the fault trace due to the variation of the acceleration. The actual recurrence rate v_F obtained from the fault database is plotted for comparison with a straight horizontal line. It is observed that the recurrence rate approximation is a conservative approach, as designed so, leading to higher rates and consequently higher fault displacement values for a given return period. This is the reason for

introducing the deterministic cap [see note (4) in Sect. 2] in order to limit the displacement estimates with respect to the fault length.

6 Summary and conclusions

Lifelines, tunnels, and bridges are vulnerable to permanent ground displacements, such as those resulting from tectonic fault movement. The estimation of the design fault displacement via empirical fault scaling relations may lead to a result of unknown safety and conservatism. On the other hand, a full Probabilistic Fault Displacement Hazard Analysis (PFDHA) is the most appropriate tool to incorporate fault productivity in terms of events per year in the calculations. PFDHA yields the mean annual frequency of exceeding predefined fault displacement values and is essentially the first step for the performance-based design of critical infrastructures. However, this approach is not compatible with the code due to the required specialized seismological data and the sophisticated calculations. To overcome these drawbacks and at the same time offer a code-compatible hazard-consistent approach, a simplified methodology for estimating the design fault displacement at lifeline–fault crossings was developed. A set of empirically-derived equations for calculating the displacement is offered given the fault productivity (as represented by the recurrence rate), the fault mechanism, the fault length, and the crossing location of the lifeline on the fault (crossing site). These equations were developed from the statistical processing of results from PFDHA by considering the pertinent epistemic uncertainties and a range of input variables, both derived and obtained, respectively, from a selection of faults from the 2020 European Fault-Source Model database (Basili et al. 2022).

The fault displacement obtained from the proposed methodology was compared to the one from a full PFDHA to a set of relevant active faults in Europe, revealing a fair match, erring towards the conservative side. The proposed methodology has been adopted as an informative Annex in prEN 1998-4:2022 (European Committee for Standardisation 2022) and it may serve as a screening tool within the lifeline route selection procedure, or as a preliminary design tool to indicate whether a specialized seismological study is needed. Finally, the methodology may be easily implemented via the spreadsheet that accompanies the paper as an electronic supplement.

7 Supplementary material

The online version contains the supplementary material.

Appendix

A1, A2, A3.

Table A1 Coefficients of Eq. (2) for normal fault mechanism

Δ_F (m)	Coeff	Recurrence rate class		Δ_F (m)	Coeff	Recurrence rate class		Δ_F (m)	Coeff	Recurrence rate class		Δ_F (m)	Coeff	Recurrence rate class	
		Low	High			Low	High			Low	High			Low	High
0.25	a_1	− 3.6511	− 0.9265	1.00	a_1	− 8.4603	− 6.3450	1.75	a_1	− 12.5074	− 10.9173	3.00	a_1	− 18.4061	− 17.9528
	a_2	0.6921	− 1.1847		a_2	2.3952	1.0138		a_2	4.0081	3.1454		a_2	6.6007	6.8172
	a_3	− 0.7924	− 8.7234		a_3	− 1.0443	− 7.5878		a_3	− 1.7911	− 7.6197		a_3	− 2.8321	− 8.2978
	a_4	− 0.2225	0.1750		a_4	− 0.4926	− 0.2241		a_4	− 0.7666	− 0.6528		a_4	− 1.2284	− 1.4322
	a_5	2.8574	6.4744		a_5	3.0686	5.9413		a_5	3.3464	5.8859		a_5	3.6840	6.1005
	a_6	− 4.8378	1.8547		a_6	− 3.6788	2.2074		a_6	− 2.5522	2.8103		a_6	− 1.2756	3.6963
	a_7	0.0139	− 0.0140		a_7	0.0291	0.0117		a_7	0.0457	0.0427		a_7	0.0748	0.1014
	a_8	− 0.3513	− 0.6960		a_8	− 0.3312	− 0.5885		a_8	− 0.3293	− 0.5536		a_8	− 0.3322	− 0.5506
	a_9	− 0.0829	− 2.1222		a_9	− 0.5931	− 2.3689		a_9	− 0.9582	− 2.5759		a_9	− 1.3206	− 2.8295
0.50	a_1	− 5.4586	− 3.0263	1.25	a_1	− 10.0535	− 8.1157	2.00	a_1	− 13.7728	− 12.4003	3.50	a_1	− 20.7246	− 20.7531
	a_2	1.3003	− 0.3635		a_2	3.0145	1.8095		a_2	4.5498	3.8982		a_2	7.6813	8.3474
	a_3	− 0.6753	− 7.9911		a_3	− 1.3295	− 7.5455		a_3	− 2.0188	− 7.7081		a_3	− 3.2224	− 8.7129
	a_4	− 0.3152	0.0316		a_4	− 0.5966	− 0.3807		a_4	− 0.8619	− 0.8109		a_4	− 1.4266	− 1.7618
	a_5	2.8847	6.1622		a_5	3.1807	5.8946		a_5	3.4242	5.9055		a_5	3.8044	6.2535
	a_6	− 4.5365	1.8317		a_6	-3.2148	2.4433		a_6	− 2.2497	2.9971		a_6	− 0.8632	4.0569
	a_7	0.0189	− 0.0053		a_7	0.0353	0.0228		a_7	0.0516	0.0545		a_7	0.0875	0.1264
	a_8	− 0.3391	− 0.6424		a_8	− 0.3299	–		a_8	− 0.3295	− 0.5490		a_8	− 0.3350	− 0.5596
	a_9	− 0.2635	− 2.1945		a_9	− 0.7496	− 2.4551		a_9	− 1.0488	− 2.6330		a_9	− 1.4273	− 2.9241

Table A1 (continued)

Δ_F (m)	Coeff	Recurrence rate class		Δ_F (m)	Coeff	Recurrence rate class		Δ_F (m)	Coeff	Recurrence rate class		Δ_F (m)	Coeff	Recurrence rate class	
		Low	High			Low	High			Low	High			Low	High
0.75	a_1	− 7.0224	− 4.7633	1.50	a_1	− 11.2729	− 9.4956	2.50	a_1	− 16.0707	− 15.1360	4.00	a_1	− 23.0154	− 23.5015
	a_2	1.8573	0.3394		a_2	3.4990	2.4528		a_2	5.5441	5.3084		a_2	8.7735	9.8655
	a_3	− 0.8239	− 7.7106		a_3	− 1.5614	− 7.5652		a_3	− 2.4315	− 7.9561		a_3	− 3.6064	− 9.1820
	a_4	− 0.4041	− 0.0962		a_4	− 0.6787	− 0.5102		a_4	− 1.0375	− 1.1088		a_4	− 1.6291	− 2.0889
	a_5	2.9716	6.0194		a_5	3.2655	5.8820		a_5	3.5581	5.9812		a_5	3.9223	6.4306
	a_6	− 4.1048	2.0057		a_6	− 2.8729	2.6267		a_6	− 1.7353	3.3418		a_6	-0.4880	4.4234
	a_7	0.0239	0.0030		a_7	0.0403	0.0322		a_7	0.0626	0.0769		a_7	0.1007	0.1512
	a_8	− 0.3338	− 0.6104		a_8	− 0.3294	− 0.5608		a_8	− 0.3304	− 0.5465		a_8	− 0.3387	− 0.5721
	a_9	− 0.4390	− 2.2858		a_9	− 0.8590	− 2.5171		a_9	− 1.1959	− 2.7326		a_9	− 1.5204	− 3.0177

Table A2 Coefficients of Eq. (2) for reverse fault mechanism

Δ_F(m)	Coeff	Recurrence rate class		Δ_F(m)	Coeff	Recurrence rate class		Δ_F(m)	Coeff	Recurrence rate class		Δ_F(m)	Coeff	Recurrence rate class	
		Low	High			Low	High			Low	High			Low	High
0.25	a_1	− 3.5809	− 0.7625	1.00	a_1	− 10.0475	− 8.6611	1.75	a_1	− 16.8189	− 17.4403	3.00	a_1	− 30.1500	− 35.2076
	a_2	0.2308	− 1.7508		a_2	2.5888	1.9420		a_2	5.7183	7.0093		a_2	12.9626	18.6243
	a_3	− 0.1928	− 8.1037		a_3	− 0.5416	− 7.9898		a_3	− 2.1580	− 10.4494		a_3	− 6.1739	− 18.9437
	a_4	− 0.1184	0.3233		a_4	− 0.4646	− 0.3807		a_4	− 1.0185	− 1.4862		a_4	− 2.4301	− 4.1774
	a_5	2.5577	6.1146		a_5	2.0486	4.5334		a_5	1.7454	3.8369		a_5	1.3568	3.9245
	a_6	− 5.1595	1.8046		a_6	2.8557	13.3393		a_6	12.4648	27.4079		a_6	31.0118	57.4639
	a_7	0.0063	− 0.0267		a_7	0.0225	0.0175		a_7	0.0552	0.0979		a_7	0.1464	0.3034
	a_8	− 0.3181	− 0.6493		a_8	− 0.1351	− 0.2240		a_8	0.0269	0.1038		a_8	0.3020	0.5877
	a_9	− 0.0133	− 2.1196		a_9	− 1.9875	− 5.0396		a_9	− 4.1008	− 8.4000		a_9	-7.9999	-15.5374
0.50	a_1	− 5.8650	− 3.5924	1.25	a_1	− 12.5237	− 11.8077	2.00	a_1	− 19.3740	− 20.8612	3.50	a_1	-36.4058	-43.5066
	a_2	0.9791	− 0.5353		a_2	3.6702	3.6747		a_2	7.0405	9.1662		a_2	16.5995	24.3589
	a_3	0.0958	− 7.4030		a_3	− 1.0989	− 8.7274		a_3	− 2.7887	− 11.6557		a_3	− 8.6270	− 24.5889
	a_4	-0.2168	0.1087		a_4	− 0.6486	− 0.7496		a_4	− 1.2687	− 1.9762		a_4	− 3.1650	− 5.5465
	a_5	2.3057	5.3286		a_5	1.9307	4.2143		a_5	1.6295	3.6812		a_5	1.3425	4.6262
	a_6	− 2.9934	5.2232		a_6	6.4181	18.3916		a_6	15.9571	32.8782		a_6	40.0859	72.8599
	a_7	0.0101	− 0.0147		a_7	0.0329	0.0437		a_7	0.0710	0.1347		a_7	0.1952	0.4106
	a_8	− 0.2507	− 0.4754		a_8	− 0.0730	− 0.0958		a_8	0.0842	0.2146		a_8	0.4155	0.7509
	a_9	− 0.6062	− 3.0354		a_9	− 2.7857	− 6.2540		a_9	− 4.8456	− 9.7000		a_9	− 9.8821	− 19.2053

Table A2 (continued)

Δ_F(m)	Coeff	Recurrence rate class		Δ_F(m)	Coeff	Recurrence rate class		Δ_F(m)	Coeff	Recurrence rate class		Δ_F(m)	Coeff	Recurrence rate class	
		Low	High			Low	High			Low	High			Low	High
0.75	a_1	− 7.9772	− 6.1239	1.50	a_1	− 14.5634	− 14.4616	2.50	a_1	− 24.3737	− 27.5073	4.00	a_1	− 42.9989	− 52.2117
	a_2	1.7541	0.6466		a_2	4.6127	5.2084		a_2	9.7104	13.4480		a_2	20.5191	30.5038
	a_3	− 0.1424	− 7.5533		a_3	− 1.6038	− 9.4959		a_3	− 4.2428	− 14.6526		a_3	− 11.5853	− 31.5342
	a_4	− 0.3311	− 0.1170		a_4	− 0.8156	− 1.0847		a_4	− 1.7842	− 2.9611		a_4	− 3.9668	− 7.0337
	a_5	2.1602	4.8702		a_5	1.8448	4.0155		a_5	1.4712	3.6458		a_5	1.4446	5.7725
	a_6	− 0.1287	9.2241		a_6	9.3248	22.6500		a_6	22.8852	43.9777		a_6	49.9537	89.8675
	a_7	0.0154	− 0.0005		a_7	0.0428	0.0682		a_7	0.1040	0.2095		a_7	0.2490	0.5283
	a_8	− 0.1904	− 0.3408		a_8	− 0.0248	0.0016		a_8	0.1886	0.4016		a_8	0.5256	0.8834
	a_9	− 1.2983	− 4.0361		a_9	− 3.4229	− 7.2690		a_9	− 6.3050	− 12.3316		a_9	− 11.9228	− 23.2660

Table A3 Coefficients of Eq. (2) for strike-slip fault mechanism

Δ_F (m)	Coeff	Recurrence rate class		Δ_F (m)	Coeff	Recurrence rate class		Δ_F(m)	coeff	Recurrence rate class		Δ_F (m)	coeff	Recurrence rate class	
		Low	High			Low	High			Low	High			Low	High
0.25	a_1	− 5.1391	− 9.3774	1.00	a_1	− 13.5015	− 11.8186	1.75	a_1	− 20.6864	− 14.1208	3.00	a_1	− 31.4180	− 17.5211
	a_2	2.2983	3.9922		a_2	6.7661	4.2274		a_2	10.6812	4.7091		a_2	16.6515	5.6120
	a_3	− 0.9885	11.1942		a_3	− 0.7515	9.7195		a_3	− 1.5496	8.7087		a_3	− 3.2521	7.8030
	a_4	− 0.6845	− 0.8118		a_4	− 1.6635	− 0.8127		a_4	− 2.5042	− 0.8686		a_4	− 3.7658	− 0.9866
	a_5	2.4665	− 1.9394		a_5	2.3699	− 1.2698		a_5	2.6156	− 0.8941		a_5	3.1914	− 0.5850
	a_6	− 2.4378	− 9.3626		a_6	− 0.7217	− 8.0084		a_6	0.6696	− 7.0357		a_6	2.2288	− 6.1299
	a_7	0.0536	0.0495		a_7	0.1265	0.0491		a_7	0.1879	0.0522		a_7	0.2786	0.0585
	a_8	− 0.2615	0.1078		a_8	− 0.2027	0.0839		a_8	− 0.1959	0.0722		a_8	− 0.2235	0.0646
	a_9	− 0.5319	1.0160		a_9	− 1.1461	0.4657		a_9	− 1.5466	0.1559		a_9	− 1.9478	− 0.1081
0.50	a_1	− 8.2578	− 10.1806	1.25	a_1	− 16.3084	− 12.7178	2.00	a_1	− 22.9875	− 14.8385	3.50	a_1	− 35.6177	− 18.8653
	a_2	3.9467	3.9855		a_2	8.2895	4.4017		a_2	11.9600	4.8859		a_2	19.0106	6.0152
	a_3	− 0.5955	10.7400		a_3	− 1.0127	9.2691		a_3	− 1.8706	8.4761		a_3	− 4.0269	7.5352
	a_4	− 1.0469	− 0.7921		a_4	− 1.9925	− 0.8321		a_4	− 2.7764	-0.8908		a_4	− 4.2601	− 1.0425
	a_5	2.3360	− 1.6912		a_5	2.4470	− 1.0983		a_5	2.7207	− 0.8113		a_5	3.4636	− 0.4996
	a_6	− 1.8781	− 8.9335		a_6	− 0.1404	− 7.5833		a_6	1.0450	− 6.8059		a_6	2.7332	− 5.8693
	a_7	0.0806	0.0479		a_7	0.1506	0.0502		a_7	0.2076	0.0534		a_7	0.3138	0.0616
	a_8	− 0.2296	0.0996		a_8	− 0.1968	0.0782		a_8	− 0.1988	0.0699		a_8	− 0.2421	0.0626
	a_9	− 0.7664	0.7988		a_9	− 1.3189	0.3268		a_9	− 1.6473	0.0862		a_9	− 2.0682	− 0.1786

Table A3 (continued)

Δ_F (m)	Coeff	Recurrence rate class		Δ_F (m)	Coeff	Recurrence rate class		Δ_F(m)	coeff	Recurrence rate class		Δ_F (m)	coeff	Recurrence rate class	
		Low	High			Low	High			Low	High			Low	High
0.75	a_1	− 10.9863	− 11.0185	1.50	a_1	− 18.4723	− 13.4162	2.50	a_1	− 27.1565	− 16.1709	4.00	a_1	− 39.7137	− 20.1969
	a_2	5.4089	4.0921		a_2	9.4655	4.5483		a_2	14.2669	5.2306		a_2	21.3144	6.4324
	a_3	− 0.6038	10.1893		a_3	− 1.2646	8.9707		a_3	− 2.5219	8.1105		a_3	-4.8251	7.2923
	a_4	− 1.3679	− 0.7991		a_4	− 2.2447	− 0.8491		a_4	− 3.2639	− 0.9353		a_4	− 4.7406	− 1.1015
	a_5	2.3303	− 1.4567		a_5	2.5248	− 0.9887		a_5	2.9392	− 0.6866		a_5	3.7467	− 0.4245
	a_6	− 1.2750	− 8.4390		a_6	0.2766	− 7.2929		a_6	1.6667	− 6.4369		a_6	3.1922	− 5.6418
	a_7	0.1046	0.0483		a_7	0.1691	0.0511		a_7	0.2427	0.0558		a_7	0.3479	0.0648
	a_8	− 0.2126	0.0907		a_8	− 0.1952	0.0749		a_8	− 0.2084	0.0670		a_8	− 0.2631	0.0606
	a_9	− 0.9722	0.6136		a_9	− 1.4379	0.2354		a_9	− 1.8084	− 0.0217		a_9	− 2.1743	− 0.2376

Supplementary Information The online version contains supplementary material available at https://doi.org/10.1007/s10518-023-01813-9.

Author's contributions VEM: Formal analysis and investigation, Conceptualization, Methodology, Writing – original draft preparation, Writing – review and editing. DV: Conceptualization, Methodology, Supervision, Writing – review and editing. LD: Conceptualization, Methodology, Writing – review and editing. RB: Methodology, Writing – review and editing.

Funding Open access funding provided by HEAL-Link Greece. The current work has been partially undertaken in as part of the Horizon 2020 Seismology and Earthquake Engineering Research Infrastructure Alliance in Europe (SERA, Grant Agreement No. 730900). The first and the second author have received partial funding from the European Union's Horizon 2020 research and innovation programme "METIS-Seismic Risk Assessment for Nuclear Safety" under Grant Agreement No. 945121 and also, the financial support provided by the Hellenic Foundation for Research and Innovation (H.F.R.I.) under the "2nd Call for H.F.R.I. Research Projects to support Faculty Members & Researchers", Project "TwinCity—Climate-Aware Risk and Resilience Assessment of Urban Areas under Multiple Environmental Stressors via Multi-Tiered Digital City Twinning" (Number: 2515) is gratefully acknowledged.

Data availability All data is available in the supplementary material.

Code availability The code is available in the supplementary material.

Declarations

Conflict of interest The authors have no conflicts of interest to declare that are relevant to the content of this article.

References

Aki K, Richards P (1980) Quantitative seismology: theory and methods. W. H. Freeman & Co, San Francisco

Anastasopoulos I, Gazetas G (2007) Foundation–structure systems over a rupturing normal fault: part I. Observations after the Kocaeli 1999 earthquake. Bull Earthq Eng 5:253–275. https://doi.org/10.1007/s10518-007-9029-2

Anastasopoulos I, Gazetas G, Bransby MF et al (2007) Fault rupture propagation through sand: finite-element analysis and validation through centrifuge experiments. J Geotech Geoenviron Eng 133(8):943–958. https://doi.org/10.1061/(ASCE)1090-0241(2007)133:8(943)

Anastasopoulos I, Gerolymos N, Gazetas G, Bransby MF (2008) Simplified approach for design of raft foundations against fault rupture. Part I: free-field. Earthq Eng Eng Vib 7:147–163. https://doi.org/10.1007/s11803-008-0835-6

Basili R, Danciu L, Beauval C, et al (2022) European Fault-Source Model 2020 (EFSM20): online data on fault geometry and activity parameters. Rome, Italy. https://doi.org/10.13127/efsm20

Basöz NI, Kiremidjian AS, King SA, Law KH (1999) Statistical analysis of bridge damage data from the 1994 Northridge, CA, earthquake. Earthq Spectra 15(1):25–54. https://doi.org/10.1193/1.1586027

Bird JF, Bommer JJ (2004) Earthquake losses due to ground failure. Eng Geol 75(2):147–179. https://doi.org/10.1016/j.enggeo.2004.05.006

Bommer JJ (2002) Deterministic vs. probabilistic seismic hazard assessment: an exaggerated and obstructive dichotomy. J Earthq Eng 6:43–73. https://doi.org/10.1080/13632460209350432

Bommer JJ, Scherbaum F (2008) The use and misuse of logic trees in probabilistic seismic hazard analysis. Earthq Spectra 24(4):997–1009. https://doi.org/10.1193/1.2977755
Casari M, Wilkie SJ (2005) Sequencing lifeline repairs after an earthquake: an economic approach. J Regul Econ 27:47–65. https://doi.org/10.1007/s11149-004-4418-9
Cornell CA, Krawinkler H (2000) Progress and challenges in seismic performance assessment. PEER Center News 3:1–4
Danciu L, Nandan S, Reyes C, et al (2021) The 2020 update of the European Seismic Hazard Model—ESHM20: Model Overview. EFEHR Technical Report 001 v1.0.0. Zurich, Switzerland. https://doi.org/10.12686/a15
Davis CA (2008) Assessing geotechnical hazards for water pipes with uniform confidence level. In: Geotechnical earthquake engineering and soil dynamics IV. ASCE, Reston, VA, pp 1–10. https://doi.org/10.1061/40975(318)194
European Committee for Standardisation (2021) EN 1998-1-1:2021, Eurocode 8: earthquake resistance design of structures—part 1–1: general rules and seismic action. Belgium, Brussels
European Committee for Standardisation (2022) prEN 1998–4:2022, Eurocode 8—design of structures for earthquake resistance—part 4: silos, tanks and pipelines, towers, masts and chimneys. Belgium, Brussels
Fragiadakis M, Vamvatsikos D, Karlaftis MG et al (2015) Seismic assessment of structures and lifelines. J Sound Vib 334(6):29–56. https://doi.org/10.1016/j.jsv.2013.12.031
Gao JC, Chan CH, Ma KF, Lee CT (2022) Probabilistic fault displacement hazards along the milun fault. Bull Seismol Soc Am 112(5):2745–2757. https://doi.org/10.1785/0120210312
Girgin S, Krausmann E (2016) Historical analysis of U.S. onshore hazardous liquid pipeline accidents triggered by natural hazards. J Loss Prev Process Ind 40:578–590. https://doi.org/10.1016/j.jlp.2016.02.008
Gutenberg R, Richter CF (1944) Frequency of earthquakes in California. Bull Seismol Soc Am 34(4):185–188. https://doi.org/10.1785/BSSA0340040185
Hamid-Mosaku IA, Oguntade OF, Ifeanyi VI et al (2020) Evolving a comprehensive geomatics multi-criteria evaluation index model for optimal pipeline route selection. Struct Infrastruct Eng 16(10):1382–1396. https://doi.org/10.1080/15732479.2020.1712435
Haver S, Winterstein SR (2009) Environmental contour lines: a method for estimating long term extremes by a short term analysis. Trans Soc Naval Archit Mar Eng 116:116–127
Honegger DG, Nyman DJ, Johnson ER et al (2004) Trans-Alaska pipeline system performance in the 2002 Denali fault, Alaska, earthquake. Earthq Spectra 20(3):707–738. https://doi.org/10.1193/1.1779239
Kilanitis I, Sextos A (2019) Integrated seismic risk and resilience assessment of roadway networks in earthquake prone areas. Bull Earthq Eng 17:181–210. https://doi.org/10.1007/s10518-018-0457-y
Kramer SL (1996) Geotechnical earthquake engineering. Prentice-Hall, Upper Saddle River
Leonard M (2014) Self-consistent earthquake fault-scaling relations: update and extension to stable continental strike-slip faults. Bull Seismol Soc Am 104(6):2953–2965. https://doi.org/10.1785/0120140087
Loukidis D, Bouckovalas GD, Papadimitriou AG (2009) Analysis of fault rupture propagation through uniform soil cover. Soil Dyn Earthq Eng 29(11–12):1389–1404. https://doi.org/10.1016/j.soildyn.2009.04.003
Mackay DJC (2005) Information theory, inference, and learning algorithms. Cambridge University Press, Cambridge
Mazumder RK, Salman AM, Li Y, Yu X (2020) Seismic functionality and resilience analysis of water distribution systems. J Pipeline Syst Eng Pract 11(1):04019045. https://doi.org/10.1061/(ASCE)PS.1949-1204.0000418
Melissianos VE, Vamvatsikos D, Gantes CJ (2017) Performance assessment of buried pipelines at fault crossings. Earthq Spectra 33(1):201–218. https://doi.org/10.1193/122015EQS187M
Melissianos VE, Danciu L, Vamvatsikos D, Basili R (2023) Fault displacement hazard estimation at lifeline–fault crossings: a simplified approach for engineering applications. Bull Earthq Eng 21:4821–4849. https://doi.org/10.1007/s10518-023-01710-1
Moss RES, Ross ZE (2011) Probabilistic fault displacement hazard analysis for reverse faults. Bull Seismol Soc Am 101(4):1542–1553. https://doi.org/10.1785/0120100248
Nair GS, Dash SR, Mondal G (2018) Review of pipeline performance during earthquakes since 1906. J Perform Constr Facil 32(6):04018083. https://doi.org/10.1061/(ASCE)CF.1943-5509.0001214
O'Rourke TD (2010) Geohazards and large, geographically distributed systems. Geotechnique 60(7):505–543. https://doi.org/10.1680/geot.2010.60.7.505
O'Rourke TD, Jeon SS, Toprak S et al (2014) Earthquake response of underground pipeline networks in Christchurch, NZ. Earthq Spectra 30(1):183–204. https://doi.org/10.1193/030413EQS062M

O'Rourke MJ, Liu JX (2012) Seismic design of buried and offshore pipelines. Monograph MCEER-12-MN04. Multidisciplinary Center for Earthquake Engineering Research, Buffalo, NY, USA

Petersen MD, Dawson TE, Chen R et al (2011) Fault displacement hazard for strike-slip faults. Bull Seismol Soc Am 101(2):805–825. https://doi.org/10.1785/0120100035

Roy N, Sarkar R (2017) A Review of seismic damage of mountain tunnels and probable failure mechanisms. Geotech Geol Eng 35:1–28. https://doi.org/10.1007/s10706-016-0091-x

Seel K, Dragan M, Coulombe-Pontbriand M, et al (2014) A spatial multi-criteria analysis process to optimize and better defend the pipeline route selection process. In: Proceedings of the 10th international pipeline conference. American society of mechanical engineers, Calgary, Alberta, Canada, p IPC201433221. https://doi.org/10.1115/IPC2014-33221

Somerville P (1995) Kobe earthquake: an urban disaster. EOS Trans Am Geophys Union 76:49–51. https://doi.org/10.1029/EO076i006p00049-02

Steinberg LJ, Cruz AM (2004) When natural and technological disasters collide: lessons from the Turkey Earthquake of August 17, 1999. Nat Hazards Rev 5:121–130. https://doi.org/10.1061/(asce)1527-6988(2004)5:3(121)

Valentini A, Fukushima Y, Contri P et al (2021) Probabilistic fault displacement hazard assessment (PFDHA) for nuclear installations according to IAEA safety standards. Bull Seismol Soc Am 111(5):2661–2672. https://doi.org/10.1785/0120210083

Wang JH (2018) A review on scaling of earthquake faults. Terr Atmos Ocean Sci 29:589–610. https://doi.org/10.3319/TAO.2018.08.19.01

Wells DL, Coppersmith KJ (1994) New empirical relationships among magnitude, rupture length, rupture width, rupture area, and surface displacements. Bull Seismol Soc Am 84(4):974–1002. https://doi.org/10.1785/BSSA0840040974

Yang S, Mavroeidis GP (2018) Bridges crossing fault rupture zones: a review. Soil Dyn Earthq Eng 113:545–571. https://doi.org/10.1016/j.soildyn.2018.03.027

Youngs RR, Coppersmith KJ (1986) Implications of fault slip rates and earthquake recurrence models to probabilistic seismic hazard estimates. Int J Rock Mech Min Sci Geomech Abstr 23:125. https://doi.org/10.1016/0148-9062(86)90651-0

Youngs RR, Arabasz WJ, Anderson RE et al (2003) A methodology for probabilistic fault displacement hazard analysis (PFDHA). Earthq Spectra 19(1):191–219. https://doi.org/10.1193/1.1542891